

Inspiralling compact objects with generic deformations

Nicholas Loutrel,¹ Richard Brito,^{2,1} Andrea Maselli,^{3,4} and Paolo Pani¹

¹*Dipartimento di Fisica, “Sapienza” Università di Roma & Sezione INFN Roma1, Piazzale Aldo Moro 5, 00185, Roma, Italy*

²*CENTRA, Departamento de Física, Instituto Superior Técnico – IST,*

Universidade de Lisboa – UL, Avenida Rovisco Pais 1, 1049 Lisboa, Portugal

³*Gran Sasso Science Institute (GSSI), I-67100 L’Aquila, Italy*

⁴*INFN, Laboratori Nazionali del Gran Sasso, I-67100 Assergi, Italy*

Self-gravitating bodies can have an arbitrarily complex shape, which implies a much richer multipolar structure than that of a black hole in General Relativity. With this motivation, we study the corrections to the dynamics of a binary system due to generic, nonaxisymmetric mass quadrupole moments to leading post-Newtonian (PN) order. Utilizing the method of osculating orbits and a multiple scale analysis, we find analytic solutions to the precession and orbital dynamics of a (generically eccentric) binary in terms of the dimensionless modulus parameters ϵ_m , corresponding to axial $m = 1$ and polar $m = 2$ corrections from oblateness/prolateness. The solutions to the precession dynamics are exact for $0 \leq \epsilon_2 < 1$, and perturbative in $\epsilon_1 \ll 1$. We further compute the leading order corrections to the gravitational wave amplitude and phase for a quasi-circular binary due to mass quadrupole effects. Making use of the stationary phase approximation and shifted uniform asymptotics (SUA), the corrections to the phase enter at relative 2PN order, while the amplitude modulations enter at -0.5PN order with a SUA amplitude correction at 3.25PN order, relative 2PN order to the leading order SUA correction. By investigating the dephasing due to generic quadrupole moments, we find that a phase difference $\gtrsim 0.1$ radians is achievable for $\epsilon_m \gtrsim 10^{-3}$, which suggests that constraints with current and future ground-based gravitational wave detectors are possible. Our results can be implemented in parameter estimation studies to constrain generic multipolar deformations of the Kerr geometry and of neutron stars.

I. INTRODUCTION

The multipolar expansion provides a powerful tool, widely used in classical field theories, to characterize the distribution of non-symmetric distributions of charges [1] and matter [2]. In General Relativity (GR) two classes of multipole moments can be defined (which are order- ℓ tensors): the mass moments $\mathcal{Q}_{\ell m}$ and the current moments $\mathcal{S}_{\ell m}$ (henceforth $|m| \leq \ell$ is the azimuthal number of the multipolar decomposition and we use units in which $G = 1$). Current moments do not have a Newtonian analogue since they are associated with the gravitational field produced by velocity fields.

Vacuum, stationary black hole (BH) solutions in GR are also asymmetric and uniquely described by the Kerr metric [3–5]. The multipole moments of a Kerr BH satisfy closed form, elegant relations

$$\begin{aligned} \mathcal{Q}_\ell &= M(ia)^\ell N_\ell \quad \ell = 2, 4, \dots \\ \mathcal{S}_\ell &= iM(ia)^\ell N_\ell \quad \ell = 1, 3, \dots, \end{aligned} \quad (1)$$

where N_ℓ is a normalization factor [6], $\mathcal{Q}_\ell \equiv \mathcal{Q}_{\ell 0}$ and $\mathcal{S}_\ell \equiv \mathcal{S}_{\ell 0}$, with $M \equiv \mathcal{Q}_0$, and $\mathcal{S}_1 \equiv aM$ being the BH’s mass and spin. Thus, the multipole moments of Eqns. (1) are entirely determined in terms of the BH’s mass and spin, as dictated by the no-hair theorems [3, 7] (see also [5, 8–11]). All other moments, namely the odd (even) ℓ -components for the mass (current) multipoles, as well as the $m \neq 0$ terms, vanish, as a consequence of axisymmetry and of equatorial symmetry.

On the other hand, the fact that all multipoles with $\ell \geq 2$ are proportional to (powers of) the spin – as

well as their specific spin dependence – is a peculiarity of the Kerr metric (although not necessarily unique to Kerr [12]). Finally, when non-spinning, any isolated BH must be spherically symmetric and described by the Schwarzschild spacetime.

The remarkable simplicity of BHs represents an exception though, not shared by other self-gravitating bodies in the Universe. For example, since no-hair theorems do not generically apply in the presence of matter, there is no compelling reason preventing a star from being arbitrarily deformed away from spherical symmetry, even when non-spinning. The Earth itself has a complex shape, different from an ellipsoid [13].

While self-gravitating perfect fluids in a static configuration do not support deviations from spherical symmetry [14], this might not be the case for elastic materials [15]. Furthermore, it was recently shown that exotic compact objects can break the symmetries of a Kerr BH and have a much richer structure [16, 17]. In particular, smoking gun evidences for the “non-Kerness” of a compact object would be given by the presence of moments that break the equatorial symmetry (e.g. the current quadrupole \mathcal{S}_2 or the mass octopole \mathcal{Q}_3 [18]), and/or the axisymmetry (e.g. a generic mass quadrupole tensor \mathcal{Q}_{2m} with three independent components, $m = 0, 1, 2$), as in the case of multipolar boson stars [19] and of fuzzball microstate geometries [20–24].

Checking whether such symmetry properties hold for an astrophysical dark object provides an opportunity to perform multiple null-hypothesis tests of the Kerr metric. The independent measurement of three multipole moments such as the mass, spin, and (axisymmetric) mass

quadrupole \mathcal{Q}_2 , would, for example, serve as a genuine strong-gravity test of the uniqueness of the Kerr family [17, 25–32]. In this context it is intriguing that current gravitational-wave (GW) observations (especially the recent GW190814 [33] and GW190521 [34, 35]) do not exclude the existence of exotic compact objects other than BHs and neutron stars. Likewise, current constraints on the spin and multipolar structure of supermassive objects coming from the Event Horizon Telescope are weak [36], and do not exclude deviations from the Kerr spacetime.

The multipolar structure of a compact object leaves a footprint within the GW signal emitted during the coalescence of a binary system, by modifying at different orders the post-Newtonian (PN) expansion used to model the waveform during the inspiral (see [37] for a review). Until recently, PN corrections coming from the multipole moments had only been computed for axial and equatorial symmetry, i.e. focusing on corrections proportional to \mathcal{Q}_2 , \mathcal{S}_3 and \mathcal{Q}_4 [25, 26, 38, 39]. Such calculations have been recently extended to include leading order corrections with broken equatorial symmetry (while preserving axisymmetry), proportional to \mathcal{S}_2 and \mathcal{Q}_3 , mostly focusing on extreme mass-ratio inspirals (EMRIs) [18].

Overall, the dominant contribution of the multipolar structure is encoded in the (typically spin-induced) mass quadrupole moment, which enters the inspiral GW phase at relative 2PN order [38]. For comparable-mass binaries, this correction is expected to be measured with percent accuracy by third-generation ground based detectors and by LISA [40–44]. The PN results also provide an order of magnitude estimate for “kludge” waveforms, used to model the long inspiral phase of an EMRI [45]. In this case it has been shown that LISA may constrain the mass quadrupole moment of the massive central object with an accuracy of one part in 10^4 [45, 46].

The aim of this paper is to extend current PN computations to binary configurations in which the compact objects show generic deformations, with no prior assumption on their underlying symmetry. We focus in particular on the leading-order corrections of the mass quadrupole tensor \mathcal{Q}_{2m} , which enter the equations of motion to leading order at relative 2PN order. When moving into an effective one-body frame, the perturbation due to mass quadrupole effects only depends on an effective mass quadrupole moment, constituting a degeneracy between the individual moments of the compact objects.

We solve for the dynamics of the binary at relative Newtonian order, specifically we consider a reduced problem where the binary is simply described by Newtonian (or the leading PN order) dynamics, and is perturbed by the 2PN order mass quadrupole effects. We use the method of osculating orbits and multiple scale analysis to solve for the leading order corrections to the dynamics of the binary. In general, the secular dynamics of the perturbation induce precession of the orbital angular momentum. Indeed, we find that alignment between the orbital angular momentum and the Z-axis of the body can only be achieved when $\mathcal{Q}_{2,\pm 1} = 0$. Defining the modulus

ϵ_m and phase α_m parameters as in Eqs. (59) and (76), we find that the secular precession equations can be solved exactly for $\epsilon_1 = 0$ and $0 \leq \epsilon_2 < 1$. Such solutions can be extended by working perturbatively in $\epsilon_1 \ll 1$.

We extend the solutions to the conservative dynamics of the binary to include radiation reaction effects through the balance laws, accounting for all of the corrections due to mass quadrupole effects. Restricting to the limit of quasi-circular binaries, we compute the corrections to the TaylorF2 waveform phase using the stationary phase approximation (SPA) [47]. Further, we include the corrections due to orbital precession using shifted uniform asymptotics (SUA), which was originally developed for spin precessing binaries in [48]. The corrections to the SPA Fourier phase enter at relative 2PN order. The amplitude modulations are controlled by the precession phase ψ_2 , which enters at absolute -0.5PN order. Meanwhile, the corrections to the SUA amplitude enters at relative 3.25PN order, which is 2PN order beyond the Newtonian order SUA corrections. A simplistic estimate of the dephasing of the waveform phase suggests that small modulus values of $\epsilon_m \sim 10^{-3}$ might be detectable with current generation interferometers, although a detailed parameter estimation study is left for future work.

The remainder of the paper is organized as follows. In Sec. II, we provide an overview of the formalism we use, and some basic details of the mathematical methods needed to solve the equations of motion. In Sec. III, we solve for the conservative dynamics of the binary, specifically the secular precession effects and the leading order orbital corrections. The solutions are broken down into the oblate/prolate (often referred to as “spheroidal” for short) case with $\epsilon_m = 0$ in Sec. III A 1, the polar case with $\epsilon_1 = 0$ and $0 \leq \epsilon_2 < 1$ in Sec. III A 2, and the axial case with $\epsilon_2 = 0$ and $\epsilon_1 \ll 1$ in Sec. III A 3. We provide the general extension of the exact polar solution to include small ϵ_1 in Sec. III A 4. In Sec. IV A, we obtain the leading order corrections to radiation reaction effects. Finally, in Sec. IV B, we compute the SUA TaylorF2 waveform for quasi-circular binaries with generic mass quadrupole effects, with the main results being the GW Fourier phase given in Eq. (134), and the GW amplitudes given in Eq. (135). Throughout this work, we use units where $G = 1$.

II. FORMALISM

A. Notation and conventions

We follow the same notation as in Ref. [49], briefly summarized here. We denote the speed of light in vacuum by c throughout the paper. Latin indices i, j, k , etc. run over three-dimensional spatial coordinates and are contracted with the Euclidean flat metric δ^{ij} . Since there is no distinction between upper and lower spatial indices, we will use only the upper ones throughout the paper. The totally antisymmetric Levi-Civita symbol is

denoted by ϵ^{ijk} . Following the STF notation [50], we use capital letters in the middle of the alphabet L, K , etc. as shorthand for multi-indices $a_1 \dots a_l, b_1 \dots b_k$, etc. Round $(\)$, square $[\]$, and angular $\langle \ \rangle$ brackets in the indices indicate symmetrization, antisymmetrization and trace-free symmetrization, respectively. For instance,

$$T^{(ab)} = T^{(ab)} - \frac{1}{3}\delta^{ab}T^{cc} = \frac{1}{2}(T^{ab} + T^{ba}) - \frac{1}{3}\delta^{ab}T^{cc}. \quad (2)$$

We call *symmetric trace-free* (STF) those tensors $T^{i_1 \dots i_l}$ that are symmetric on all indices and whose contraction of any two indices vanishes

$$\begin{aligned} T^{(i_1 \dots i_l)} &= T^{i_1 \dots i_l}, \\ T^{i_1 \dots i_k i_k \dots i_l} &= 0, \\ T^{\langle i_1 \dots i_l \rangle} &= T^{i_1 \dots i_l}. \end{aligned} \quad (3)$$

The contraction of a STF tensor T^L with a generic tensor U^L is $T^L U^L = T^L U^{\langle L \rangle}$. For a generic vector u^i we define $u^{ij \dots k} \equiv u^i u^j \dots u^k$ and $u^2 \equiv u^{ii}$. Derivatives with respect to the coordinate time t are expressed by over-dots.

For a generic body A , the mass and current STF multipole tensors are denoted by Q_A^L and S_A^L , respectively. Restricted to a two-body system, $A = 1, 2$, we define the mass ratios $\eta_A = M_A/M$, where $M = M_1 + M_2$ is the total mass and M_A is the mass monopole; $M_A = Q_A$ in the Newtonian limit. The symmetric mass ratio is $\nu = \eta_1 \eta_2$ and the reduced mass is $\mu = \nu M$. We define the dimensionless spin parameters $\chi_A = c S_A / (\eta_A M)^2$, where $S_A = \sqrt{S_A^i S_A^i}$ is the absolute value of the current dipole moment. The body position, velocity and acceleration vectors are denoted by $z_A^i, v_A^i = \dot{z}_A^i$ and $a_A^i = \ddot{z}_A^i$, respectively. We define the two-body relative position, velocity and acceleration vectors by $z^i = z_2^i - z_1^i, v^i = v_2^i - v_1^i$ and $a^i = a_2^i - a_1^i$, respectively. We also define the relative unit vector $n^i = z^i/r$, where $r = \sqrt{z^i z^i}$ is the orbital distance. Using these definitions the radial velocity is given by $\dot{r} = v^i n^i$. Finally, for a binary system in circular orbit we define the PN expansion parameter $\tilde{u} = (2\pi F M)^{1/3}/c$, where F is the orbital frequency. Note that $\tilde{u} = v + \mathcal{O}(c^{-4})$.

B. Main equations

The post-Newtonian Lagrangian describing the two-body interaction, up to the relevant multipole moments, can be written as

$$\mathcal{L} = \mathcal{L}_{\text{pp}} + \mathcal{L}_{\text{spin}} + \mathcal{L}_{\text{quad}}. \quad (4)$$

Here, \mathcal{L}_{pp} describes the PN interaction between two point particles of mass m_1 and m_2 , which up to 2PN order is given in relative coordinates

$$\mathcal{L}_{\text{pp}} = \mathcal{L}_{\text{N}} + c^{-2}\mathcal{L}_{1\text{PN}} + c^{-4}\mathcal{L}_{2\text{PN}} + \mathcal{O}(c^{-6}), \quad (5)$$

with

$$\mathcal{L}_{\text{N}} = \frac{1}{2}\mu v^2 + \frac{\mu M}{r} \quad (6)$$

and the higher PN order terms given in Appendix A. The term $\mathcal{L}_{\text{spin}}$ contains the contributions from current dipoles, specifically the spin angular momenta of each body, and is given to second order in spins by [51]

$$\begin{aligned} \mathcal{L}_{\text{spin}} &= \frac{1}{2}\eta_1 \eta_2 \epsilon^{ijk} v^i a^j \Sigma^k + \frac{2M}{r^2} \eta_1 \eta_2 \epsilon^{ijk} v^i n^j (S^k + \Sigma^k) \\ &\quad - \frac{3}{r^3} S_1^i S_2^j n^{\langle ij \rangle}, \end{aligned} \quad (7)$$

where $S^i = S_1^i + S_2^i$ and $\Sigma^i = (\eta_2/\eta_1)S_1^i + (\eta_1/\eta_2)S_2^i$, with $S_{1,2}^i$ the spin angular momenta of each body. Finally, the mass quadrupole contribution reads, to leading PN order [49],

$$\mathcal{L}_{\text{quad}} = \frac{3M}{2r^3} Q_{\text{eff}}^{ij} n^{\langle ij \rangle} + \mathcal{O}(c^{-2}), \quad (8)$$

where $Q_{\text{eff}}^{ij} = \eta_2 Q_1^{ij} - \eta_1 Q_2^{ij}$, with $Q_{1,2}^{ij}$ the mass quadrupole moments of each body. In the following we shall ignore the tidal deformability of the bodies, which corresponds to the part of the Lagrangian describing the internal dynamics.

In the case of a binary system, the dynamics in the center-of-mass (COM) frame is described by the orbital separation $z^i = z_2^i - z_1^i$. From the variation of the above Lagrangian with respect to the worldline coordinates $z_{1,2}^i$ we can derive the equations of motion of the binary:

$$\begin{aligned} a^i &= \ddot{z}^i = \ddot{z}_2^i - \ddot{z}_1^i \\ &= a_{\text{pp}}^i + a_{\text{spin}}^i + a_{\text{quad}}^i. \end{aligned} \quad (9)$$

The mass and spin contributions are

$$\begin{aligned} a_{\text{pp}}^i &= -\frac{M}{r^2} n^i + a_{1\text{PN}}^i + a_{2\text{PN}}^i + \mathcal{O}(c^{-5/2}), \quad (10) \\ a_{\text{spin}}^i &= \frac{1}{r^3} \left\{ 6n^i [\epsilon^{jkp} n^k v^p (S^j + \Sigma^j)] \right. \\ &\quad \left. - \epsilon^{ijk} [v^j (4S^k + 3\Sigma^k) + 3\dot{r} n^j (2S^k + \Sigma^k)] \right\} \\ &\quad + \frac{15}{\mu r^4} S_1^j S_2^k n^{\langle ijk \rangle} + \mathcal{O}(c^{-5/2}), \end{aligned} \quad (11)$$

whereas the mass quadrupole contribution is

$$a_{\text{quad}}^i = -\frac{15Q_{\text{eff}}^{\langle jk \rangle}}{2\nu r^4} n^{\langle ijk \rangle} + \mathcal{O}(c^{-6}). \quad (12)$$

The orbital equations of motion must be supplemented by a suitable set of equations describing the dynamics of the spin angular momenta of each body. There are two ways of achieving this, through the fluid description of PN sources [2] or through effective field theory [52]. Both methods give the same result, namely

$$\frac{dS_1^i}{dt} = \epsilon^{ijk} \left[\Omega^j S_1^k + \mathcal{T}_{\text{QM}}^{jk} \right], \quad (13)$$

velocities are

$$r_K = \frac{p}{1 + e \cos V}, \quad (23)$$

$$\dot{r}_K = e \left(\frac{M}{p} \right)^{1/2} \sin V, \quad (24)$$

$$\dot{\phi}_K = \left(\frac{M}{p^3} \right)^{1/2} (1 + e \cos V)^2, \quad (25)$$

where e is the Newtonian orbital eccentricity, p is the semi-latus rectum, and $V = \phi - \omega$ is the true anomaly, with ω the longitude of pericenter. In the absence of a perturbing force, the motion of the binary is planar. However, this is not necessarily true in the perturbed case, and we need to generalize the prescription of the orbit further. Defining a new frame spanned by the vectors $[\hat{e}_X, \hat{e}_Y, \hat{e}_Z]$, the orbit can be arranged into an arbitrary orientation with respect to this new frame through the use of Euler angles, as illustrated in Fig. 1. A sufficient parameterization is [2]

$$\hat{n} = [\cos \Omega \cos \phi - \cos \iota \sin \Omega \sin \phi, \sin \Omega \cos \phi + \cos \iota \cos \Omega \sin \phi, \sin \iota \sin \phi], \quad (26)$$

$$\hat{\lambda} = [-\cos \Omega \sin \phi - \cos \iota \sin \Omega \cos \phi, -\sin \Omega \sin \phi + \cos \iota \cos \Omega \cos \phi, \sin \iota \cos \phi], \quad (27)$$

$$\hat{L} = [\sin \iota \sin \Omega, -\sin \iota \cos \Omega, \cos \iota], \quad (28)$$

where ι is the inclination angle and Ω is the longitude of the ascending node. The Keplerian orbit is now parameterized by five conserved quantities $\mu^a = [p, e, \iota, \omega, \Omega]$.

The method of osculating orbits posits that, under the action of any perturbing force, the parameters μ^a are no longer constant, but vary in time according to the perturbing force. The trajectory of the binary is parameterized by $\vec{r} = \vec{r}(t, \mu^a)$ and $\vec{v} = \vec{v}(t, \mu^a)$, while the equations of motion are

$$\frac{d}{dt} \vec{r}(t, \mu^a) = \vec{v}(t, \mu^a), \quad (29)$$

$$\frac{d}{dt} \vec{v}(t, \mu^a) = \vec{f}_N + \vec{f}_{\text{pert}}, \quad (30)$$

with \vec{f}_{pert} the perturbing force. The method of osculating

orbits promotes the conserved parameters to functions of the time variable, specifically $\mu^a \rightarrow \mu^a(t)$, and thus

$$\frac{d}{dt} = \frac{\partial}{\partial t} + \frac{d\mu^a}{dt} \frac{\partial}{\partial \mu^a}. \quad (31)$$

The first term above generates the usual conserved Keplerian orbits, while the remaining equations are

$$\frac{d\mu^a}{dt} \frac{\partial \vec{r}}{\partial \mu^a} = 0, \quad (32)$$

$$\frac{d\mu^a}{dt} \frac{\partial \vec{v}}{\partial \mu^a} = \vec{f}_{\text{pert}}(\mu^a). \quad (33)$$

Specifying the perturbing force as $\vec{f}_{\text{pert}} = \mathcal{R}\hat{n} + \mathcal{S}\hat{\lambda} + \mathcal{W}\hat{L}$, the osculating equations for μ^a are [2]

$$\frac{dp}{dt} = 2 \left(\frac{p^3}{M} \right)^{1/2} \frac{\mathcal{S}}{1 + e \cos V}, \quad (34)$$

$$\frac{de}{dt} = \left(\frac{p}{M} \right)^{1/2} \left[\sin V \mathcal{R} + \frac{2 \cos V + e(1 + \cos^2 V)}{1 + e \cos V} \mathcal{S} \right], \quad (35)$$

$$\frac{d\iota}{dt} = \left(\frac{p}{M} \right)^{1/2} \frac{\cos(V + \omega)}{1 + e \cos V} \mathcal{W}, \quad (36)$$

$$\frac{d\Omega}{dt} = \left(\frac{p}{M} \right)^{1/2} \frac{\sin(V + \omega)}{1 + e \cos V} \frac{\mathcal{W}}{\sin \iota}, \quad (37)$$

$$\frac{d\omega}{dt} = \frac{1}{e} \left(\frac{p}{M} \right)^{1/2} \left[-\cos V \mathcal{R} + \frac{2 + e \cos V}{1 + e \cos V} \sin V \mathcal{S} - e \cot \iota \frac{\sin(V + \omega)}{1 + e \cos V} \mathcal{W} \right]. \quad (38)$$

Note that there are only five parameters μ^a , but Eqs. (32)-(33) are six equations in total. The five equations for μ^a are supplemented by an additional equation

for the true anomaly V in order to complete this system of equations. Such equation is given by $\dot{V} = \dot{\phi}_K - (\dot{\omega} + \dot{\Omega} \cos \iota)$, which uses the above equations for ω

and Ω . The action of the perturbing force on the orbit is now fully specified.

When studying the evolution of the osculating equations, it is important to realize that they depend on at least two timescales, the orbital timescale encoded through the dependence on V and a secular timescale, which is determined by the perturbing force. In order to obtain PN accurate solutions, we must then solve the osculating equations using multiple scale analysis [2] (in this case, two timescale analysis). Because the equations are parameterized in terms of V rather than t , it is convenient to recast them as $d\mu^a/dV = (d\mu^a/dt)/(dV/dt)$ and PN expand to the relevant order. The two scales of the problem then become V which is the shorter scale, and $\tilde{V} := \epsilon V$ the longer scale, where $f_{\text{pert}}^i = \mathcal{O}(\epsilon)$ with ϵ an order keeping parameter. The derivative operator then becomes,

$$\frac{d}{dV} = \frac{\partial}{\partial V} + \epsilon \frac{\partial}{\partial \tilde{V}}, \quad (39)$$

and our ansatz for the solution is

$$\mu^a = \mu_0^a(\tilde{V}) + \epsilon \mu_1^a(V, \tilde{V}) + \mathcal{O}(\epsilon^2). \quad (40)$$

The leading order term above μ_0^a is only dependent on the long secular scale \tilde{V} , since the μ^a are conserved for unperturbed Keplerian orbits.

The strategy to solve the osculating equations is to combine Eqs. (39) – (40) with Eqs. (34) – (38), and expand to the relevant order in ϵ . The leading order equation is

$$\frac{d\mu_0^a}{d\tilde{V}} + \frac{\partial \mu_1^a}{\partial V} = \mathcal{F}^a(V; \mu_0^a), \quad (41)$$

where \mathcal{F}^a are given by the right hand side of Eqs. (34) – (38). This equation can be solved by realizing that the dependence on the shorter scale V is purely oscillatory. Upon averaging in the following fashion,

$$\langle f \rangle = \frac{1}{2\pi} \int_0^{2\pi} f(V) dV, \quad (42)$$

Eq. (41) reduces to

$$\frac{d\mu_0^a}{d\tilde{V}} = \langle \mathcal{F}^a \rangle(\mu_0^a), \quad (43)$$

which uniquely determines μ_0^a . Finally, to obtain μ_1^a , we combine Eq. (43) with Eq. (41) and integrate with respect

to V , specifically

$$\mu_1^a(V, \tilde{V}) = \mu_{1,\text{sec}}^a(\tilde{V}) + \int dV [\mathcal{F}^a(V; \mu_0^a) - \langle \mathcal{F}^a \rangle(\mu_0^a)]. \quad (44)$$

This determines μ_1^a up to a purely secular term $\mu_{1,\text{sec}}^a(\tilde{V})$, which is determined by next order equations in ϵ . For the purposes of the present calculation, it suffices to stop the analysis here.

III. GENERIC MASS QUADRUPOLE EFFECTS

The perturbing force we desire to investigate is given in Eq. (12), which is dependent on the effective quadrupole tensor Q_{eff}^{ij} . In order to calculate the necessary components of the perturbing force for the osculating equations, we need to specify the components of this STF tensor. To do so, we assume the quadrupole moment is held fixed with respect to the (XYZ) -frame, which we now refer to as the body frame. For convenience, this frame is also chosen such that the direction of the total angular momentum J^i is aligned with the Z -directions e_Z^i . In this frame, the STF tensor can be readily decomposed into spherical harmonics, specifically

$$Q_{\text{eff}}^{<ij>} = W_2 \sum_{m=-2}^2 \mathcal{Y}_{2m}^{<ij>} Q_m, \quad (45)$$

where Q_m are the spherical harmonic coefficients of the mass quadrupole, $\mathcal{Y}_{lm}^{<L>}$ are defined as

$$\mathcal{Y}_{lm}^{<L>} = \frac{1}{W_l} \int dS^2 N^{<L>} Y_{lm}^\dagger(\theta, \phi), \quad (46)$$

with $N^i = [\sin \theta \cos \phi, \sin \theta \sin \phi, \cos \theta]$, $Y_{lm}(\theta, \phi)$ the spherical harmonic functions, $W_l = 4\pi l!/(2l+1)!!$, and the integral is performed over the 2-sphere. Note that in general, the Q_m 's are complex (except when $m=0$) while the components of $Q^{<ij>}$ are real. It is thus simpler to specify the components of $Q^{<ij>}$ in terms of the real and imaginary parts of the Q_m 's, specifically

$$Q_{+1} = Q_{+1}^R + iQ_{+1}^I, \quad (47)$$

$$Q_{+2} = Q_{+2}^R + iQ_{+2}^I. \quad (48)$$

The decomposition for the negative m terms follows from $Q_{-m} = (-1)^m Q_m^\dagger$, while Q_0 is real valued. With this, the osculating equations for the mass quadrupole correction become

$$\left\langle \frac{dt}{dt} \right\rangle = \left(\frac{6\pi}{5} \right)^{1/2} \frac{(1-e^2)^{3/2}}{\nu M^{1/2} p^{7/2}} \left\{ \cos \iota (-Q_{+1}^R \cos \Omega + Q_{+1}^I \sin \Omega) + \sin \iota [Q_{+2}^R \sin(2\Omega) + Q_{+2}^I \cos(2\Omega)] \right\}, \quad (49)$$

$$\left\langle \frac{d\Omega}{dt} \right\rangle = \left(\frac{\pi}{5} \right)^{1/2} \frac{(1-e^2)^{3/2}}{\nu M^{1/2} p^{7/2}} \left\{ \cos \iota [3Q_0 + \sqrt{6}Q_{+2}^R \cos(2\Omega) - \sqrt{6}Q_{+2}^I \sin(2\Omega)] + \sqrt{6} \cos(2\iota) \csc \iota (Q_{+1}^R \sin \Omega + Q_{+1}^I \cos \Omega) \right\}, \quad (50)$$

$$\left\langle \frac{d\omega}{dt} \right\rangle = \frac{1}{4} \left(\frac{\pi}{5} \right)^{1/2} \frac{(1-e^2)^{3/2}}{\nu M^{1/2} p^{7/2}} \left\{ -3Q_0 [3 + 5 \cos(2\iota)] + 2\sqrt{6} [3 - 5 \cos(2\iota)] \cot \iota (Q_{+1}^R \sin \Omega + Q_{+1}^I \cos \Omega) \right. \\ \left. + \sqrt{6} [1 - 5 \cos(2\iota)] (Q_{+2}^R \cos(2\Omega) - Q_{+2}^I \sin(2\Omega)) \right\}, \quad (51)$$

while $[e, p]$ do not change on the secular timescale to leading order and are determined by Eq. (44).

The above osculating equations are actually equivalent to Eq. (20), describing the precession of the orbital angular momentum L^i around the total angular momentum J^i . In order for the direction of J^i to be conserved, one also has to consider the precession of the spins, which after orbit averaging Eq. (13) become

$$\left\langle \frac{dS_1^i}{dt} \right\rangle = -\frac{3\eta_2 M}{2p^3} (1-e^2)^{3/2} \epsilon^{ijk} Q_1^{<ja>} \hat{L}^{<ka>}, \quad (52)$$

$$\left\langle \frac{dS_2^i}{dt} \right\rangle = -\frac{3\eta_1 M}{2p^3} (1-e^2)^{3/2} \epsilon^{ijk} Q_2^{<ja>} \hat{L}^{<ka>}. \quad (53)$$

For the present calculations, we will neglect the spin-orbit and spin-spin effects when considering the precession induced by quadrupole effects. The reason for this is that the PN precession equations up to the relevant PN order have only recently been solved analytically in the case when Q^{ij} corresponds to the spin-induced quadrupole moment [53–56]. The case for generic Q^{ij} has not been solved. For simplicity, we shall consider only nonspinning binaries and hence neglect the relativistic spin-orbit and spin-spin couplings. In such a scenario, the problem reduces down to first solving Eqs. (49)-(51), and then solving the above spin precession equations for $S_{1,2}^i$. In the following sections we consider the generic problem of solving the osculating equations.

As a special application of the system of equations given by Eqs. (49)-(51) and Eqs. (52)-(53), we consider the case where \hat{L}^i and $S_{1,2}^i$ are aligned with the Z-direction of the body frame in Sec. III B.

A. Precessing Solutions

Consider the problem of solving Eqs. (49)-(51). In general, there does not appear to be a closed-form analytic solution to this system for generic non-zero quadrupole coefficients $[Q_0, Q_{+1}^{R,I}, Q_{+2}^{R,I}]$ and $\iota \neq 0$. However, there are some special configurations which allow for closed-form solutions. The three cases are as follows:

- Spheroidal: $Q_{\pm 1} = 0 = Q_{\pm 2}$ with Q_0 non-vanishing
- Polar: $Q_{\pm 1} = 0$ with $[Q_0, Q_{\pm 2}]$ non-vanishing
- Axial: $Q_{\pm 2} = 0$ with $[Q_0, Q_{\pm 1}]$ non-vanishing

Below, we detail each of these cases.

1. Spheroidal Case

The spheroidal case considers the scenario where the compact object has an oblate/prolate spheroidal shape, and thus the only non-vanishing quadrupole coefficients is the $m = 0$ term. A common astrophysical scenario that would create such an effect is a quadrupole moment induced by rotation. For the calculation at hand, we leave Q_0 as a generic constant. However, in the case of spin-induced quadrupole moment, $Q_0 = C_Q \chi^2 M^3 + \mathcal{O}(\chi^4)$ with χ the dimensionless spin parameter, M the mass of the compact object, and a proportionality factor C_Q which is dependent on the equation of state. In the Kerr BH case, $C_Q = -1$ and higher-order spin corrections in Q_0 vanish identically.

In this scenario, the secular equations simplify to

$$\left\langle \frac{d\iota}{dt} \right\rangle = 0, \quad (54)$$

$$\left\langle \frac{d\Omega}{dt} \right\rangle = 3 \left(\frac{\pi}{5} \right)^{1/2} \frac{(1-e^2)^{3/2}}{\nu M^{1/2} p^{7/2}} Q_0 \cos \iota, \quad (55)$$

$$\left\langle \frac{d\omega}{dt} \right\rangle = -\frac{3}{4} \left(\frac{\pi}{5} \right)^{1/2} \frac{(1-e^2)^{3/2}}{\nu M^{1/2} p^{7/2}} Q_0 [3 + 5 \cos(2\iota)]. \quad (56)$$

As can be seen from Eq. (54), the inclination angle becomes constant, and thus, there is no nutation. The only effect on the binary is the precession of the orbital plane, encoded through $[\Omega, \omega]$. Taking $\iota = \iota_0 = \text{const.}$, and defining

$$\frac{d\psi_0}{dt} = 3 \left(\frac{\pi}{5} \right)^{1/2} \frac{Q_0 (1-e^2)^{3/2}}{\nu M^{1/2} p^{7/2}} \cos \iota_0, \quad (57)$$

Eqs. (55)-(56) can be directly integrated to obtain

$$\Omega = \psi_0, \quad \omega = -\frac{1}{4} \sec \iota_0 [3 + 5 \cos(2\iota_0)] \psi_0. \quad (58)$$

Note that here we wrote the solutions in terms of the dependent variable ψ_0 instead of time. The reason for this is that the right hand side of Eq. (57) is function of the orbital velocity through $[p, e]$ and will thus change on the radiation reaction timescale. We expand on this more in Sec. IV A.

2. Polar Case

The polar case is named due to the fact that the non-vanishing quadrupole coefficients $[Q_0, Q_{\pm 2}]$ correspond to spherical harmonics modes that are even under spatial reflection, i.e. polar modes. In this scenario,

it is convenient to define the dimensionless parameters $\tau_2 = Q_{+2}^R/Q_0$ and $i_2 = Q_{+2}^I/Q_0$. Further, we define the *polar modulus* ϵ_2 and *polar argument* α_2 such that

$$\epsilon_2 = \left[\frac{2}{3} (\tau_2^2 + i_2^2) \right]^{1/2}, \quad \alpha_2 = \frac{1}{2} \tan^{-1} (i_2/\tau_2). \quad (59)$$

Finally, we define ψ_2 such that

$$\frac{d\psi_2}{dt} = 3 \left(\frac{\pi}{5} \right)^{1/2} \frac{Q_0(1 - e^2)^{3/2}}{\nu M^{1/2} p^{7/2}} \sqrt{1 - \epsilon_2^2 \cos \iota}. \quad (60)$$

Unlike the spheroidal case, the inclination angle is no longer constant and the primary effect of the $m = \pm 2$ modes is to induce nutation of the orbital angular momentum. As a result, the above definition for ψ_2 no longer varies on solely the radiation reaction timescale, but also on the precession timescale through ι . Also, note the presence of ϵ_2 in Eq. (60), as opposed to Eq. (57) since $\epsilon_2 = 0$ in the spheroidal case.

The starting point for solving the secular equations in this case is to divide Eq. (50) by Eq. (60). Defining $\mathcal{V} = \Omega + \alpha_2$, we arrive at

$$\frac{d\mathcal{V}}{d\psi_2} = \frac{1 + \epsilon_2 \cos(2\mathcal{V})}{\sqrt{1 - \epsilon_2^2}}. \quad (61)$$

The solution to this equation depends on the value of ϵ_2 , which depends on the specific scenario under consideration. For astrophysical objects, the induction of a quadrupole moment on the body is largely expected to be a result of spin angular momentum creating an $m = 0$ contribution. However, such objects are also likely not perfectly spheroidal, but may have small deviations on their surface (e.g. mountains on a neutron star) which could contribute to $|m| > 0$ modes [15]. Such contributions are expected to be small, and we could thus assume that $\epsilon_2 \ll 1$.

Another example of how to generate an $|m| > 0$ mode on a compact object is through dynamical tides. A sufficiently rapid change in the electric tidal moment $G_{ij} = \partial_{ij}U$, with U the Newtonian potential, can excite f-modes on the surface of any compact object, e.g. [57]. In the case of a spin-aligned binary, this will generate f-modes with $m = 0$ and $m = \pm 2$. In this case, the amplitude of the f-modes are 2PN order, i.e. they scale like $\mathcal{O}(v^4)$ with v the orbital velocity. Thus, these effects are potentially subdominant compared to an intrinsic spheroidness, and we may once again assume $\epsilon_2 \ll 1$.

Finally, a further example are deformed BHs in modified gravity, where uniqueness and no-hair theorems might not hold.¹

¹ Although such deformed solutions exist (e.g., [58, 59]) they arise from modified field equations that also affect the binary dynamics in other ways (e.g. by extra dissipative terms). Since we assume GR, our approach can describe this situation only if beyond-GR effects to the dynamics (e.g. modified fluxes) are negligible compared to the multipolar deformations.

To be as general as possible while still working in the realm of astrophysical plausibility, we take $0 \leq \epsilon_2 < 1$ for the remainder of this calculation. Under this assumption, the solution to Eq. (61) is

$$\mathcal{V} = \tan^{-1} \left[\sqrt{\frac{1 + \epsilon_2}{1 - \epsilon_2}} \tan \psi_2 \right]. \quad (62)$$

Such an expression should be familiar to anyone who has studied Keplerian orbits, since it takes the same form as the mapping between the true anomaly V and the eccentric anomaly u for eccentric binaries, specifically

$$\frac{V}{2} = \tan^{-1} \left[\sqrt{\frac{1 + e}{1 - e}} \tan \left(\frac{u}{2} \right) \right]. \quad (63)$$

These expressions have known issues with branch cuts when $[\psi_2, u/2] = n\pi/2$ with n an integer. However, it has been shown [60] through trigonometric identities that an equivalent expression that removes the branch cuts and properly tracks the secular behavior of V with increasing u is

$$V = u + 2 \tan^{-1} \left(\frac{\beta_e \sin u}{1 - \beta_e \cos u} \right), \quad (64)$$

where

$$\beta_e = \frac{1 - \sqrt{1 - e^2}}{e}. \quad (65)$$

Thus, an equivalent expression for $\mathcal{V}(\psi_2)$ can be found by taking $V \rightarrow 2\mathcal{V}$ and $u \rightarrow 2\psi_2$, specifically

$$\mathcal{V} = \psi_2 + \tan^{-1} \left[\frac{\beta_2 \sin(2\psi_2)}{1 - \beta_2 \cos(2\psi_2)} \right], \quad (66)$$

where $\beta_2 = \beta_e(e \rightarrow \epsilon_2)$.

Moving on to the inclination angle, we proceed by dividing Eq. (49) by Eq. (60), and then divide by Eq. (61), to obtain

$$\frac{d\iota}{d\mathcal{V}} = \frac{\epsilon_2}{\sqrt{1 - \epsilon_2^2}} \left[\frac{\tan \iota \sin(2\mathcal{V})}{1 + \epsilon_2 \cos(2\mathcal{V})} \right]. \quad (67)$$

Such an equation can be directly integrated to obtain

$$\frac{\sin \iota}{\sin \iota_0} = \sqrt{\frac{1 + \epsilon_2}{1 + \epsilon_2 \cos(2\mathcal{V})}}, \quad (68)$$

where ι_0 is the initial value of the inclination angle, i.e. $\iota_0 = \iota(\mathcal{V} = 0)$. Using Eq. (62), this can be re-written in terms of ψ_2 as the dependent variable, specifically

$$\frac{\sin \iota}{\sin \iota_0} = \sqrt{\frac{1 + \epsilon_2 \cos(2\psi_2)}{1 + \epsilon_2}}. \quad (69)$$

Note that in the limit $\iota_0 \rightarrow 0$, the orbital angular momentum vector becomes aligned with the Z -axis of the

body frame and ι becomes a constant. Thus, in the limit of alignment, there is no nutation.

Finally, moving on to the longitude of pericenter, we obtain an equation for $d\omega/d\psi_2$ by dividing Eq. (51) by Eq. (60). After some manipulation, this equation takes the form

$$\frac{d\omega}{d\psi_2} = -\frac{c_1 + c_2 \cos(2\psi_2)}{[1 - \epsilon_2 \cos(2\psi_2)]\sqrt{a_- - b \cos(2\psi_2)}}, \quad (70)$$

where

$$a_{\pm} = 1 \pm \epsilon_2 - \sin^2 \iota_0, \quad (71)$$

$$b = -\epsilon_2 \sin^2 \iota_0, \quad (72)$$

$$c_1 = 3 - \epsilon_2 (5 + 4\epsilon_2) + 5(1 + \epsilon_2) \cos(2\iota_0), \quad (73)$$

$$c_2 = \epsilon_2 (1 + 5\epsilon_2) - 5\epsilon_2 (1 + \epsilon_2) \cos(2\iota_0). \quad (74)$$

Naturally, this equation can be directly integrated to obtain

$$\omega - \omega_0 = \frac{\sec \iota_0}{4\sqrt{1 - \epsilon_2^2}} \left[\frac{c_2}{\epsilon_2} \text{EllF} \left(\psi_2 \middle| \frac{2b}{b - a_-} \right) - 4(1 + \epsilon_2) \text{EllI} \left(\frac{2\epsilon_2}{1 - \epsilon_2}; \psi_2 \middle| \frac{2b}{b - a_-} \right) \right], \quad (75)$$

where ω_0 is the initial value, EllF and EllI are the elliptic integrals of the first and third kind, respectively. Note that this equation is divergent in the limit $\iota_0 \rightarrow \pi/2$, since ω becomes ill-defined in this limit.

We leave the calculation of the solution to Eq. (60) to the discussion in Sec. IV A.

3. Axial Case

The axial case is defined as the situation when $Q_{\pm 2}$ are zero, while the $Q_{\pm 1}$ coefficients are non-zero, which correspond to spherical harmonic modes that are odd under parity. Much of the setup for this case is the same as the polar case. We define the dimensionless parameters $\mathbf{r}_1 = Q_{+1}^R/Q_0$ and $\mathbf{i}_1 = Q_{+1}^I/Q_0$, from which we can define the *axial modulus* and *axial argument*,

$$\epsilon_1 = \left[\frac{2}{3} (\mathbf{r}_1^2 + \mathbf{i}_1^2) \right]^{1/2}, \quad \alpha_1 = \tan^{-1} (\mathbf{i}_1/\mathbf{r}_1). \quad (76)$$

We also modify the definition of ψ_2 to obtain ψ_1 , specifically

$$\frac{d\psi_1}{dt} = 3 \left(\frac{\pi}{5} \right)^{1/2} \frac{Q_0(1 - e^2)^{3/2}}{\nu M^{1/2} p^{7/2}} \sqrt{1 - \epsilon_1^2 \cos \iota}. \quad (77)$$

Lastly, we define $\mathcal{V} = \Omega + \alpha_1$. With these new variables, the relevant equations become

$$\frac{d\iota}{d\psi_1} = -\frac{\epsilon_1 \cos \mathcal{V}}{\sqrt{1 - \epsilon_1^2}}, \quad (78)$$

$$\frac{d\mathcal{V}}{d\psi_1} = \frac{1 + 2\epsilon_1 \cot(2\iota) \sin \mathcal{V}}{\sqrt{1 - \epsilon_1^2}}, \quad (79)$$

$$\frac{d\omega}{d\psi_1} = \frac{-5 \cos \iota + \sec \iota + \epsilon_1 [3 - 5 \cot(2\iota)] \csc \iota \sin \mathcal{V}}{2\sqrt{1 - \epsilon_1^2}}. \quad (80)$$

Unlike the polar case, the evolution of \mathcal{V} is not decoupled from the evolution of ι . It makes sense then to divide Eq. (78) by Eq. (79) to obtain $d\iota/d\mathcal{V}$. Further, we make the change of variables $\gamma = \cot \iota$, which gives

$$\frac{d\gamma}{d\mathcal{V}} = \frac{\gamma(1 + \gamma^2)\epsilon_1 \cos \mathcal{V}}{\gamma - (1 - \gamma^2)\epsilon_1 \sin \mathcal{V}}. \quad (81)$$

This equation has a known exact solution, specifically

$$\gamma = (1 + \gamma_0^2)\epsilon_1 \sin \mathcal{V} + \sqrt{\gamma_0^2 + (1 + \gamma_0^2)^2 \epsilon_1^2 \sin^2 \mathcal{V}}, \quad (82)$$

where $\gamma_0 = \cot \iota_0$ with $\iota_0 = \iota(\mathcal{V} = 0)$.

With the solution for ι in hand, one can insert this into Eqs. (79)-(80) and try to solve for $[\mathcal{V}, \omega]$. Unfortunately, there does not appear to be a closed form solution to these for arbitrary value of ϵ_1 , even if we enforce the condition $\epsilon_1 < 1$. We instead solve the equations perturbatively in $\epsilon_1 \ll 1$, which is the case of most relevance to astrophysical scenarios. A straightforward calculation gives

$$\mathcal{V}(\psi_1) = \psi_1 + \sum_{n=1}^{\infty} \epsilon_1^n \mathcal{V}_{(n)}(\psi_1), \quad (83)$$

$$\omega(\psi_1) - \omega_0 = \frac{1 - 4\gamma_0^2}{2\gamma_0 \sqrt{1 + \gamma_0^2}} \psi_1 + \sum_{n=1}^{\infty} \epsilon_1^n \omega_{(n)}(\psi_1), \quad (84)$$

with ω_0 and integration constant, and the first few functions in each sum given below,

$$\mathcal{V}_{(1)} = -\frac{2}{\gamma_0} (1 - \gamma_0^2) \sin^2(\psi_1/2), \quad (85)$$

$$\mathcal{V}_{(2)} = \frac{5}{2} \psi_1 - \frac{(1 - \gamma_0^2)}{\gamma_0^2} \sin \psi_1 - \frac{(1 + \gamma_0^4)}{2\gamma_0^2} \sin(2\psi_1), \quad (86)$$

$$\omega_{(1)} = \frac{(1 - 2\gamma_0^2 + 2\gamma_0^4)}{2\gamma_0^2 \sqrt{1 + \gamma_0^2}} \cos \psi_1, \quad (87)$$

$$\begin{aligned} \omega_{(2)} = & -\frac{(1 - 6\gamma_0^2 + 28\gamma_0^4)}{8\gamma_0^3 \sqrt{1 + \gamma_0^2}} \psi_1 \\ & + \frac{(1 - 3\gamma_0^2 - 4\gamma_0^4 + 2\gamma_0^6)}{2\gamma_0^3 \sqrt{1 + \gamma_0^2}} \sin \psi_1 \\ & - \frac{(3 - 8\gamma_0^2 - 4\gamma_0^4 - 8\gamma_0^6)}{16\gamma_0^3 \sqrt{1 + \gamma_0^2}} \sin(2\psi_1). \end{aligned} \quad (88)$$

Note that the above solutions properly reduce to Eq. (58) in the limit $\epsilon_1 \rightarrow 0$.

4. Toward a General Solution

Having considered the scenarios where analytic solutions are possible, some of which are in closed form, we

may now work toward constructing general solutions to Eqs. (49)-(51). We showed in Sec. III A 2 that the case with $\epsilon_1 = 0$ and $\epsilon_2 \neq 0$ admits closed form solutions. We choose to study the construction of a general solution by starting with the closed form solutions of Sec. III A 2 and consider the axial effects as a perturbation. The ansatz for the general solution will be

$$\sin \iota = \sin [\iota_2(\psi_2)] + \sum_{n=1}^{\infty} \epsilon_1^n I_{(n)}(\psi_2), \quad (89)$$

$$\Omega + \alpha_2 = \mathcal{V}_2(\psi_2) + \sum_{n=1}^{\infty} \epsilon_1^n V_{(n)}(\psi_2), \quad (90)$$

$$\omega - \omega_0 = \omega_2(\psi_2) + \sum_{n=1}^{\infty} \epsilon_1^n W_{(n)}(\psi_2), \quad (91)$$

where $[\Omega_0, \omega_0]$ are integration constants, and $\sin \iota_2$, \mathcal{V}_2 , and ω_2 are given as functions of ψ_2 in Eqs. (69),(66),

and (75), respectively. To obtain the relevant equations for $\Lambda_{(n)}^a = [I_{(n)}, V_{(n)}, W_{(n)}]$, we insert the above ansatz into Eq. (49)-(51), and expand about $\epsilon_1 \ll 1$.

To order $\mathcal{O}(\epsilon_1^0)$, the osculating equations are automatically satisfied. To higher order, we obtain equations of the schematic form

$$\frac{d\Lambda_{(n)}^a}{d\psi_2} = F_{(n)}^a \left[\psi_2, \Lambda_{(1)}^b(\psi_2), \dots, \Lambda_{(n-1)}^b(\psi_2); \epsilon_2 \right]. \quad (92)$$

In practice, we have failed to find closed form solutions to these equations for arbitrary ϵ_2 , and have instead sought to solve them in the limit $\epsilon_2 \ll 1$. The solutions take the general form of a power series, specifically

$$\Lambda_{(n)}^a = \sum_{k=0}^{\infty} \epsilon_2^k \Lambda_{(n,k)}^a(\psi_2). \quad (93)$$

Defining $\Delta = \alpha_1 - \alpha_2$, the solutions up to order $\mathcal{O}(\epsilon_1 \epsilon_2)$ are

$$I_{(1,0)} = -2 \cos \iota_0 \cos \left(\Delta + \frac{\psi_2}{2} \right) \sin \left(\frac{\psi_2}{2} \right), \quad (94)$$

$$I_{(1,1)} = \frac{1}{6} \sec \iota_0 \sin \left(\frac{\psi_2}{2} \right) \{ 6 \cos \psi_2 \sin \Delta - \cos(2\iota_0) [-6 \sin \Delta + 9 \sin(\Delta - \psi_2) + 5 \sin(\Delta + \psi_2) + 10 \sin(\Delta + 2\psi_2)] \}, \quad (95)$$

$$V_{(1,0)} = -2 \cot(2\iota_0) [\cos \Delta - \cos(\Delta + \psi_2)], \quad (96)$$

$$V_{(1,1)} = \frac{1}{48} \{ 4 [9 + 10 \cos(2\iota_0) + 5 \cos(4\iota_0)] \csc \iota_0 \sec^3 \iota_0 \sin \Delta \sin^3 \psi_2 + \cos \Delta \sec \iota_0 [-48 \cos(2\iota_0 \cos(2\psi_2)) \csc \iota_0 + 3(-7 + 10 \cos[2\iota_0] + 5 \cos[4\iota_0]) \cos \psi_2 \csc \iota_0 \sec^2 \iota_0 + (9 + 10 \cos[2\iota_0] + 5 \cos[4\iota_0]) \cos(3\psi_2) \csc \iota_0 \sec^2 \iota_0 + (2 + \cos[2\iota_0]) \sec \iota_0 \tan \iota_0 \} \}, \quad (97)$$

$$W_{(1,0)} = \frac{1}{8} \sec \iota_0 \tan \iota_0 \left\{ 2\psi_2 \sin \Delta [7 + 5 \cos(2\iota_0)] - \csc^2 \iota_0 [7 + 4 \cos(2\iota_0) + 5 \cos(4\iota_0)] \sin \left(\Delta + \frac{\psi_2}{2} \right) \sin \left(\frac{\psi_2}{2} \right) \right\}, \quad (98)$$

$$W_{(1,1)} = \frac{1}{576} \csc \iota_0 \sec^4 \iota_0 \left\{ \cos \Delta \left[-2(11 - 323 \cos[2\iota_0] + 65 \cos[4\iota_0] + 55 \cos[6\iota_0]) + 36(2 + \cos[2\iota_0])(3 - 16 \cos[2\iota_0] + 5 \cos[4\iota_0]) \cos \psi_2 + 9(12 + 35 \cos[2\iota_0] + 12 \cos[4\iota_0] + 5 \cos[6\iota_0]) \cos(2\psi_2) - (14 + 7 \cos[2\iota_0] + 50 \cos[4\iota_0] + 25 \cos[6\iota_0]) \cos(3\psi_2) \right] + \sin \Delta \left[9(-2 - 37 \cos[2\iota_0] + 2 \cos[4\iota_0] + 5 \cos[6\iota_0]) \sin \psi_2 + 6 \sin^2 \iota_0 (\psi_2 [131 + 188 \cos\{2\iota_0\} + 65 \cos\{4\iota_0\}] + 3[3 + \cos\{2\iota_0\}] [-1 + 5 \cos\{2\iota_0\}]) \sin[2\psi_2] + (14 + 7 \cos[2\iota_0] + 50 \cos[4\iota_0] + 25 \cos[6\iota_0]) \sin(4\psi_2) \right] \right\}. \quad (99)$$

We stop the expansion here since the solutions for $\Lambda_{(n,k)}^a$ become increasingly complicated. The above discussion and results present a schematic of the calculation, and one can easily extend these results to higher order in $\epsilon_{1,2}$ if desired.

To provide an estimate of the accuracy of the above solutions, we compare these analytic results to numeri-

cal evolutions of Eqs. (49)-(51). In order to perform the numerical integration of the equations, we convert them to equations of the form $d\mu^a/d\psi_2$, and recast them in terms of $\epsilon_{1,2}$ and $\alpha_{1,2}$ instead of the Q_m coefficients. We set $\epsilon_2 = 0.9$, $\alpha_2 = 0$, $\alpha_1 = \pi/2$, and study the behavior of the solutions for different values of ϵ_1 , specifically $\epsilon_1 = [10^{-7}, 10^{-5}, 10^{-3}]$. The results of this comparison

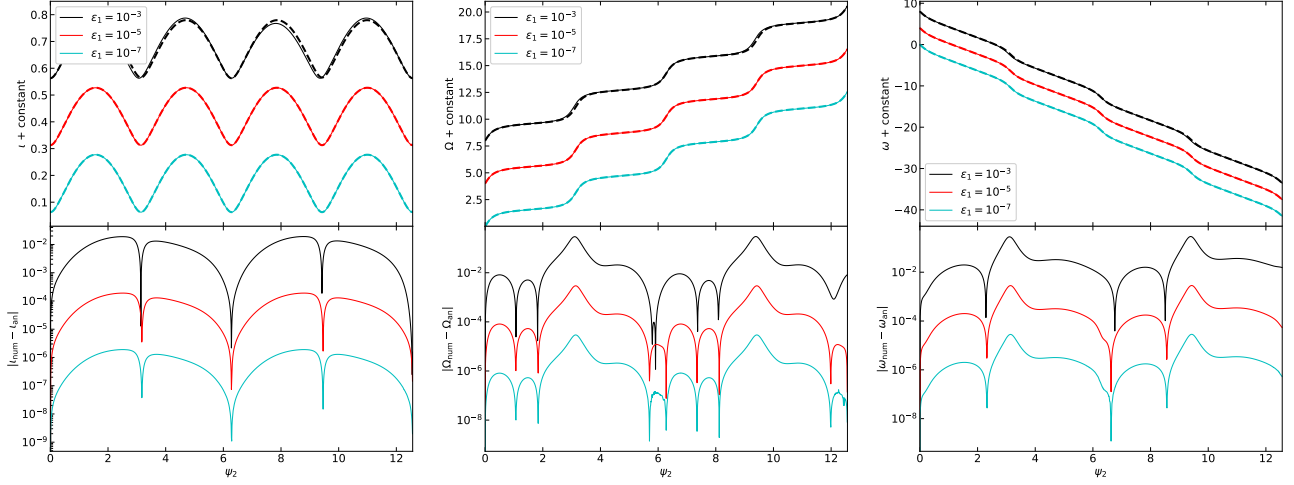


FIG. 2. Top Panel: Comparison of the numerical evolution of ι (left), Ω (middle), and ω (right) from Eqs. (49)-(51) (solid lines) to the analytic solutions (dashed lines) given in Sec. III A 4 for $\epsilon_2 = 0.9$, $\alpha_2 = 0$, $\alpha_1 = \pi/2$. Each color represents a different value of ϵ_1 , specifically 10^{-3} (black/upper), 10^{-5} (red/middle), and 10^{-7} (cyan/lower). All of the calculations are performed with $\iota_0 = \pi/50$. Each case is offset by a constant value from the others so that they do not overlap. Bottom Panels: Relative difference between the numeric and analytic solutions.

are shown in Fig. 2. The top panels show the plots of both the numeric (solid lines) and analytic (dashed lines) for (from left to right) ι , Ω , and ω . The bottom panels display the relative difference between the two solutions, showing the error introduced in each phase. As ϵ_1 decreases by each order of magnitude, so does the error by a comparable amount. Note that this has to be the case since the analytic solutions are exact in the limit $\epsilon_1 \rightarrow 0$.

B. Non-precessing Solutions

Alignment between the Z -axis of the body frame and \hat{L} , specifically $\iota = 0$ and $\langle d\iota/dt \rangle = 0$, is only possible when $Q_{\pm 1} = 0$. When this occurs, the orbital basis of Eqs. (26)-(28) reduces down to

$$\hat{n} = [\cos(\phi + \Omega), \sin(\phi + \Omega), 0], \quad (100)$$

$$\hat{\lambda} = [-\sin(\phi + \Omega), \cos(\phi + \Omega), 0], \quad (101)$$

$$\hat{L} = [0, 0, 1], \quad (102)$$

and thus the effect of the mass quadrupole contributions is to modulate the orbital phase ϕ by Ω .

The solutions in this limit can be considered as a special class of the polar solutions. Defining $[\psi_2, \epsilon_2, \alpha_2]$ as in Eqs. (59) and (60), it follows that $\mathcal{V} = \Omega + \alpha_2$ still obeys Eq. (66). The longitude of pericenter reduces to

$$\omega - \omega_0 = -\frac{1}{\sqrt{1 - \epsilon_2^2}} \left[\psi_2 + (1 + \epsilon_2) \Pi \left(\frac{2\epsilon_2}{1 - \epsilon_2}; \psi_2 \middle| 0 \right) \right]. \quad (103)$$

A straightforward calculation shows that the direction of

pericenter advances at the constant rate

$$\lim_{\iota \rightarrow 0} \left(\frac{d\omega}{d\psi_2} + \cos \iota \frac{d\Omega}{d\psi_2} \right) = -\frac{1}{\sqrt{1 - \epsilon_2^2}}. \quad (104)$$

The motion in the aligned limit is now fully specified.

C. Oscillatory Effects & Orbital Motion

As mentioned at the beginning of this section, $\langle de/dt \rangle = 0 = \langle dp/dt \rangle$, and thus the leading order correction to $[e, p]$ comes from the oscillatory effects of Eq. (44). In order to complete our solution to the dynamics of the binary to leading order in the mass quadrupole moment (or alternatively, complete to 2PN order), we must also consider these oscillatory effects in $[e, p]$. We do not need to consider these corrections to the angles $[\iota, \Omega, \omega]$, since these terms do not enter relevant orbital quantities until relative 2PN order, and thus their oscillatory effects will be further suppressed to relative 4PN order. Following Eq. (44), the solutions for $[e, p]$ are schematically

$$e(V) = e_0 + \frac{1}{p_0^2} \sum_{k=0} [C_k^e \cos(kV) + \mathcal{S}_k^e \sin(kV)] + \mathcal{O}(p_0^{-4}), \quad (105)$$

$$\frac{p(V)}{p_0} = 1 + \frac{1}{p_0^2} \sum_k [C_k^p \cos(kV) + \mathcal{S}_k^p \sin(kV) + \mathcal{O}(p_0^{-4})], \quad (106)$$

where $[e_0, p_0]$ are determined by initial conditions. We do not provide the specific $[C_k, \mathcal{S}_k]$ coefficients in this work, since they are rather long and unenlightening. However, they can be readily computed from Eqs. (34)-(35).

Naively, one might expect that e_0 would correspond to the actual (in a geometric sense) eccentricity of the orbit, and likewise for the semi-latus rectum p_0 . However, this is not in general true. Indeed, one can easily check that $e_0 = 0$ does not correspond to circular orbits, since $\lim_{e_0 \rightarrow 0} e(V) \neq 0$. We, thus, have to redefine these parameters such that they make physical sense. To do this, we follow [61], and define the new eccentricity and semi-latus rectum as

$$\tilde{e} = \frac{\sqrt{\Omega_p} - \sqrt{\Omega_a}}{\sqrt{\Omega_p} + \sqrt{\Omega_a}}, \quad (107)$$

$$\tilde{p} = M \left(\frac{2}{\sqrt{M\Omega_p} + \sqrt{M\Omega_a}} \right)^{4/3}, \quad (108)$$

where $[\Omega_p, \Omega_a] = [\max dV/dt, \min dV/dt]$. The resulting expressions are

$$\tilde{e} = e_0 + \sqrt{\frac{\pi}{5}} \frac{1}{8\nu M p_0^2} \sum_a Q^a \tilde{\mathcal{E}}_a(\iota, \Omega, \omega) + \mathcal{O}(p_0^{-4}), \quad (109)$$

$$\tilde{p} = p_0 \left[1 + \sqrt{\frac{\pi}{5}} \frac{1}{3\nu M p_0^2} \sum_a Q^a \tilde{\mathcal{P}}_a(\iota, \Omega, \omega) + \mathcal{O}(p_0^{-4}) \right], \quad (110)$$

where $Q^a = [Q_0, Q_1^{R,I}, Q_2^{R,I}]$, and the coefficients $[\tilde{\mathcal{E}}_a, \tilde{\mathcal{P}}_a]$ are given in Appendix B. This allows us to now properly take the circular limit $\tilde{e} \rightarrow 0$, since that is the limit of most relevance to ground based GW detectors. For the remainder of the calculation, we work in this limit.

In the next section, we will calculate the leading order effects due to radiation reaction on the binary, but in order to complete that, we need two more quantities from the orbital dynamics, namely the modifications to Kepler's third law and the on-shell orbital energy. The former of these allows us to relate the orbital velocity to the orbital frequency. To do so, we begin by calculating the corrections to the orbital period, which is computed by

$$T_{\text{orb}} = \int_0^{2\pi} \left(\frac{dV}{dt} \right)^{-1} dV. \quad (111)$$

The orbital frequency is then $F = 1/T_{\text{orb}}$. With the orbital velocity $v = \tilde{p}\dot{\phi}$ in the limit $\tilde{e} = 0$, we obtain

$$v = \tilde{u} \left[1 + \frac{\tilde{u}^4}{72\nu M^3} \sqrt{\frac{\pi}{5}} \sum_a Q^a \tilde{\Omega}_a(\iota, \Omega, \omega) + \mathcal{O}(\tilde{u}^8) \right], \quad (112)$$

where $\tilde{u} = (2\pi M F)^{1/3}$ and the coefficients $\tilde{\Omega}_a$ are given in Appendix B.

Lastly, we need the on-shell orbital energy in order to utilize the balance law for radiation reaction. The starting point is Eq. (16), including only the Newtonian and quadrupole terms. To evaluate this on shell, one

has to insert Eqs. (23)-(25) into this to write E_{orb} in terms of the osculating quantities μ^a . This expression is still dependent on the orbital timescale through V . To address this, we then have to combine this expression with Eqs. (105)-(106) and truncate at the relevant PN order. The final result, which is independent of V , is

$$E_{\text{orb}} = -\frac{1}{2}\mu\tilde{u}^2 \left[1 + \frac{\tilde{u}^4}{36\nu M^3} \sqrt{\frac{\pi}{5}} \sum_a Q^a \tilde{E}_a(\iota, \Omega, \omega) + \mathcal{O}(\tilde{u}^8) \right] \quad (113)$$

where we have made use of Eqs. (109)-(110), and taken the limit $\tilde{e} \rightarrow 0$. The coefficients \tilde{E}_a are also given in Appendix B.

It is worth noting that all of the orbital quantities derived in this section vary on the precessing timescale through $[\iota, \Omega, \omega]$. We discuss in detail how to handle this behavior in the next section.

IV. GW EMISSION

The solutions of the previous section constitute the solutions to the conservative dynamics of the binary in the presence of generic mass quadrupole effects. In this section, we will consider the effects of dissipation on such systems through the emission of GWs.

A. Radiation reaction

We wish to compute the leading PN order corrections to the inspiral of compact binaries due to generic quadrupole effects. In order to do so, it suffices to consider the leading PN order effects in radiation reaction, which are governed by the quadrupole approximation. The energy \mathcal{P} and angular momentum \mathcal{J}^i fluxes due to GWs therein are governed by

$$\mathcal{P} = \frac{1}{5c^5} \ddot{I}^{\langle ij \rangle} \ddot{I}^{\langle ij \rangle}, \quad (114)$$

$$\mathcal{J}^i = \frac{2}{5c^5} \epsilon^{ijk} \ddot{I}^{\langle jq \rangle} \ddot{I}^{\langle kq \rangle}, \quad (115)$$

with I^{ij} the orbital quadrupole moment of the binary. The quadrupole deformation of the body does not explicitly contribute to these equations since we are assuming that the Q_m 's are static. However, they do contribute implicitly through the definition of I^{ij} , specifically

$$I^{ij} = \mu x^i x^j + \mathcal{O}(c^{-2}), \quad (116)$$

where r is given by Eq. (23) and n^i is given by Eq. (26). Due to the osculating nature of the orbit, when taking the time derivatives of I^{ij} , we must act on the elements $[\iota, \omega, \Omega]$ in addition to the orbital phase ϕ . For each time derivative acting on the former, we are required to insert the osculating equations in Eqs. (36)-(38), and then accurately PN truncate them.

In the present calculation, we take the limit $\tilde{\epsilon} = 0$, since most binaries of relevance to ground based detectors will have negligible eccentricity. We then calculate the rate of change of the orbital energy, which is related to the energy flux through the balance law

$$\frac{dE_{\text{orb}}}{dt} = -\langle \mathcal{P} \rangle, \quad (117)$$

and where E_{orb} is given by Eq. (16). Since we only desire the leading PN order correction, it suffices to work at relative Newtonian order, meaning we only need to consider the contributions E_{N} and E_{quad} when using Eq. (16).

We must begin by evaluating Eq. (114). The time derivative can be performed by acting on Eq. (116) directly. The one important feature of said procedure is that every time an instance of the acceleration $a^i = \ddot{x}^i$ appears, we must insert the equations of motion in Eq. (9). Since we are working to relative Newtonian order, it suffices to only consider the Newtonian and mass quadrupole terms in the relative acceleration equation. Doing so, we end up with $\ddot{I}^{ij} = \ddot{I}_0^{ij} + \delta(\ddot{I}^{ij})$, where

$$\ddot{I}_0^{ij} = \mu M \left[\frac{6\dot{r}}{r^4} x^i x^j - \frac{8}{r^3} v^{(i} x^{j)} \right], \quad (118)$$

$$\delta(\ddot{I}^{ij}) = 2\mu \left[2f_{\text{pert}}^{(i} v^{j)} + \dot{f}_{\text{pert}}^{(i} x^{j)} \right], \quad (119)$$

where f_{pert}^i is given by Eq. (12). The energy flux can now be directly computed using Eqs. (23)-(28). When taking the orbit average necessary for the balance law, we must also take into account the corrections to the orbital period and dV/dt , both of which are detailed in Sec. III C.

On the other hand, the orbital energy is given in Eq. (113). When taking a time derivative of this expression, one has to remember that now \tilde{u} is being promoted to a function of time. The orbital energy also depends on μ^a , and one would need to insert the osculating equations $d\mu^a/dt$ everywhere these terms appear. However, we are only working to relative Newtonian order, so these will introduce higher PN order effects that we may neglect. Thus, we are left with only terms depending on $d\tilde{u}/dt$ in Eq. (117). Solving, we obtain

$$\frac{d\tilde{u}}{dt} = \frac{32}{5} \frac{\nu}{M} \tilde{u}^9 \left[1 + \frac{\tilde{u}^4}{8M^3\nu} \sqrt{\frac{\pi}{5}} \sum_a Q^a \tilde{U}_a(\iota, \Omega, \omega) \right] \quad (120)$$

where the coefficients \tilde{U}_a are given in Appendix B. We now have the necessary equation to solve for the evolution of the binary under radiation reaction.

In general, radiation reaction introduces a new timescale to the problem, in addition to the orbital timescale encoded in V and the precession timescale encoded in ψ_2 . To consistently solve the problem, one has to, once again, solve the relevant equations in a multiple scale analysis, now with three timescales. As we detailed back in Sec. II C, the leading order behavior is obtained by averaging over the relevant oscillatory scales. In the

process of deriving Eq. (120), we already performed the average over the oscillatory orbital timescale. Observe that the coefficients \tilde{U}_a only depend on ψ_2 through oscillatory functions of $[\iota, \Omega, \omega]$. Thus, the precession effects in Eq. (120) are actually oscillatory effects, and it suffices to perform a precession average, i.e.

$$\langle f \rangle_{\psi_2} = \frac{1}{2\pi} \int_0^{2\pi} f(\psi_2) d\psi_2. \quad (121)$$

We will thus obtain double averaged equations that constitute the leading order behavior under radiation reaction. The precession average of Eq. (120) is found by simply making the replacement $U_a \rightarrow \langle U_a \rangle_{\psi_2}$. In general, the averages do not admit closed form expressions for arbitrary $\epsilon_{1,2}$. Given the astrophysical considerations discussed in Sec. III A, we compute these in an expansion $\epsilon_1 \ll 1 \gg \epsilon_2$, which provides us the mapping

$$\sum_a Q^a \langle \tilde{U}_a \rangle_{\psi_2} \rightarrow Q_0 \sum_{pq} \epsilon_1^p \epsilon_2^q \mathcal{U}_{pq}(\iota_0, \omega_0, \alpha_1, \alpha_2) \quad (122)$$

where the coefficients only depend on constants of the precession dynamics and are listed in Appendix B. For brevity, we will drop the explicit sum over $[p, q]$ and apply the Einstein summation convention in future expressions.

In order to compute the Fourier domain gravitational waveform through the SPA, we require three phases, namely $[t(\tilde{u}), \phi(\tilde{u}), \psi_2(\tilde{u})]$. The first of these is found by inverting $\langle d\tilde{u}/dt \rangle_{\psi_2}$, specifically

$$\begin{aligned} t(\tilde{u}) &= t_c + \int d\tilde{u} \left(\left\langle \frac{d\tilde{u}}{dt} \right\rangle_{\psi_2} \right)^{-1} \\ &= t_c - \frac{5M}{256\nu\tilde{u}^8} \left[1 - \frac{Q_0\tilde{u}^4}{4M^3\nu} \sqrt{\frac{\pi}{5}} \epsilon_1^p \epsilon_2^q \mathcal{U}_{pq} \right] \end{aligned} \quad (123)$$

where t_c is the time of coalescence. Similarly, the orbital phase is $d\phi/dt = \tilde{u}^3/M$, and thus

$$\begin{aligned} \phi(\tilde{u}) &= \phi_c + M^{-1} \int d\tilde{u} \tilde{u}^3 \left(\left\langle \frac{d\tilde{u}}{dt} \right\rangle_{\psi_2} \right)^{-1} \\ &= \phi_c - \frac{1}{32\nu\tilde{u}^5} \left[1 - \frac{5Q_0\tilde{u}^4}{8M^3\nu} \sqrt{\frac{\pi}{5}} \epsilon_1^p \epsilon_2^q \mathcal{U}_{pq} \right] \end{aligned} \quad (124)$$

where ϕ_c is the phase of coalescence.

The evolution of the precession phase $\psi_2(\tilde{u})$ requires more careful consideration. The time evolution of ψ_2 is given in Eq. (60). Unlike the functions $[t(\tilde{u}), \phi(\tilde{u})]$ where we could average over ψ_2 , we cannot do so here and must consider the full evolution equations $d\psi_2/d\tilde{u}$, which is obtained by dividing Eq. (60) by Eq. (120). However, since the evolution of ψ_2 is already of linear order in the mass quadrupole moments and of absolute 2PN order, it suffices for our purposes to truncate this expression to leading PN order, obtaining

$$\frac{d\psi_2}{d\tilde{u}} = \frac{3\sqrt{5\pi}}{32} \frac{Q_0\sqrt{1-\epsilon_2^2}}{M^2\nu\tilde{u}^2} \cos \iota, \quad (125)$$

where ι is a function of ψ_2 through Eq. (89). We solve this perturbatively in $\epsilon_1 \ll 1$, while keeping ϵ_2 arbitrary, just as we did in Sec. III A 4. Writing $\psi_2(\tilde{u}) = \psi_{2,0}(\tilde{u}) + \epsilon_1 \psi_{2,1}(\tilde{u}) + \mathcal{O}(\epsilon_1^2)$, we obtain to leading order

$$\frac{d\psi_{2,0}}{d\tilde{u}} = \frac{3\sqrt{5\pi}}{32} \frac{Q_0 \sqrt{1 - \epsilon_2}}{M^2 \nu \tilde{u}^2} [a_+ + b \cos(2\psi_2)]^{1/2}. \quad (126)$$

This expression can be directly integrated by moving all terms dependent on ψ_2 to the left hand side and integrating. The resulting integral on the left hand side produces the elliptic integral of the first kind $\text{EllF}[\psi_2 | 2b/(b+a_+)]$. Despite the dependence on specialized functions, the resulting equality can be solved to obtain $\psi_{2,0}(\tilde{u})$ by utilizing the fact that the Jacobi amplitude function $\text{am}(x|n)$ is the inverse of the elliptic integral of the first kind, specifically $\text{am}[\text{EllF}(x|n)|n] = x$. Rearranging, we obtain

$$\psi_{2,0}(\tilde{u}) = \text{am} \left[\text{EllF} \left(\psi_c \left| \frac{2b}{b+a_+} \right. \right) - \Psi_2(\tilde{u}) \left| \frac{2b}{b+a_+} \right. \right] \quad (127)$$

where a_+ is given in Eq. (71), and

$$\Psi_2(\tilde{u}) = \frac{3\sqrt{5\pi}}{32} \frac{Q_0 \sqrt{1 - \epsilon_2^2}}{M^2 \nu \tilde{u}} \cos \iota_0. \quad (128)$$

This expression is exact in the limit $\epsilon_1 \rightarrow 0$, and for $\epsilon_2 \in [0, 1)$. Note that $\Psi_2 \sim \tilde{u}^{-1}$, and is thus a -0.5PN effect, unlike the orbital phase in Eq. (124) which scales as \tilde{u}^{-5} and enters at -2.5PN order.

The correction to the precession phase $\psi_{2,1}(\tilde{u})$ due to axial modes require a more in depth calculation. Similar to the results in Sec. III A 4, there does not appear to be a closed form solution to this for arbitrary ϵ_2 , and we instead solve them in the limit $\epsilon_2 \ll 1$. To leading order,

$$\frac{d\psi_{2,1}}{d\tilde{u}} = \frac{3\sqrt{5\pi}}{16} \frac{Q_0 \sin \iota_0}{M^3 \nu} \left\{ \frac{\sin[\Delta + \psi_c - \Psi_0(\tilde{u})] - \sin \Delta}{2\tilde{u}^2} \right\}. \quad (129)$$

where $\Psi_0 = \lim_{\epsilon_2 \rightarrow 0} \Psi_2$. This can be directly integrated to obtain

$$\psi_{2,1}(\tilde{u}) = \sin \Delta \tan \iota_0 \Psi_0(\tilde{u}) - \tan \iota_0 \cos[\Delta + \psi_c - \Psi_0(\tilde{u})] + \mathcal{O}(\epsilon_2). \quad (130)$$

The calculation can be extended to include the $\mathcal{O}(\epsilon_2^n)$ corrections to $\psi_{2,1}(\tilde{u})$ in a straightforward way. We do not calculate them here for brevity, as well as the fact that these terms will scale as $\epsilon_1 \epsilon_2^n$ in the precession phase, and can thus be treated as higher order.

In Fig. 3, we compare the analytic approximation of $t(\tilde{u})$, $\phi(\tilde{u})$, $\psi_2(\tilde{u})$ derived in this section to numerical evolutions of the precessions equations in Eqs. (36) coupled to Eqs. (120) to include radiation reaction. For these numerical evolutions, we fixed $\epsilon_1 = 10^{-3}$ and varied $\epsilon_2 = [10^{-3}, 10^{-2}, 10^{-1}]$. In doing so, we found that the dephasing between the two solutions, which encodes the error in the analytic expressions, depends on ϵ_1 only

mildly. For $t(\tilde{u})$ and $\phi(\tilde{u})$, the dephasing becomes of order one radian for the largest value of ϵ_2 . The dephasing for these quantities can be improved by carrying the $\epsilon_1 \ll 1 \gg \epsilon_2$ expansion to higher order. On the other hand, the dephasing in $\psi_2(\tilde{u})$ does not vary significantly for varying ϵ_2 , since it can be solved for exactly in the case of polar configurations.

B. Gravitational waveform

Let us now consider the gravitational waveform of a binary with arbitrary mass quadrupole coefficients. For simplicity, we will seek to develop the corrections to the TaylorF2 waveforms for quasi-circular binaries due to generic mass quadrupoles. To derive this, it suffices to consider the quadrupole approximation, where the metric perturbation is given by

$$h_{ij} = \frac{2}{c^4 D_L} \ddot{I}_{\langle ij \rangle}, \quad (131)$$

where D_L is the luminosity distance to the source. The orbital quadrupole moment must be handled in the manner described above Eq. (118) when working in the osculating formalism. The observable waveform is found by projecting h_{ij} into the transverse trace-less (TT) gauge. In order to do this, we define the line of sight vector $N^i = [\sin \theta_N \cos \phi_N, \sin \theta_N \sin \phi_N, \cos \theta_N]$, where θ_N is the angle between the Z-axis of the body frame and N^i , and ϕ_N is the angle that the projection of N^i makes in the XY-plane with the X-axis. We consider these angles to be constant in the observer's frame. The projection into the TT gauge can be performed via Eq. (11.44) in [2], which gives us the following plus and cross polarizations for the waveform,

$$h = h_+ - ih_\times = \frac{\nu M}{D_L} \tilde{u}^2 \sum_{mn} A_{m,n}(\iota, \Omega) e^{in\phi} {}_{-2}Y_{2m}(\theta_N, \phi_N) \quad (132)$$

where ${}_{-2}Y_{lm}(\theta, \phi)$ are spin weight -2 spherical harmonics, m is an integer such that $|m| \leq 2$ and $n = \pm 2$. The amplitude functions $A_{m,n}$ are listed in Appendix C.

Since the binary is precessing, the amplitudes A_{mn} depend on time through $[\iota, \Omega]$. In order to calculate the Fourier domain waveform, we make use of the SPA and SUA [48] to obtain the precession corrections. The phase of the Fourier integral is of the standard form $\Psi_F = 2\pi f t(\tilde{u}) + n\phi(\tilde{u})$, and the stationary point is given by $\tilde{u}_* = \tilde{u}(t_*) = (-2\pi M f / n)^{1/3}$. Note that this only contributes to the Fourier transform for positive frequencies for $n = -2$. The SUA corrections are found through $T_n = 1/\sqrt{n\ddot{\phi}(\tilde{u}_*)}$. After applying both the SPA and SUA corrections, the resulting waveform is

$$\tilde{h}(f) = \sqrt{\frac{5}{96}} \frac{\mathcal{M}^{5/6}}{\pi^{2/3} D_L} f^{-7/6} e^{i\tilde{\Psi}_F} \sum_m \mathcal{A}_m(f) {}_{-2}Y_{2m}(\theta_N, \phi_N) \quad (133)$$

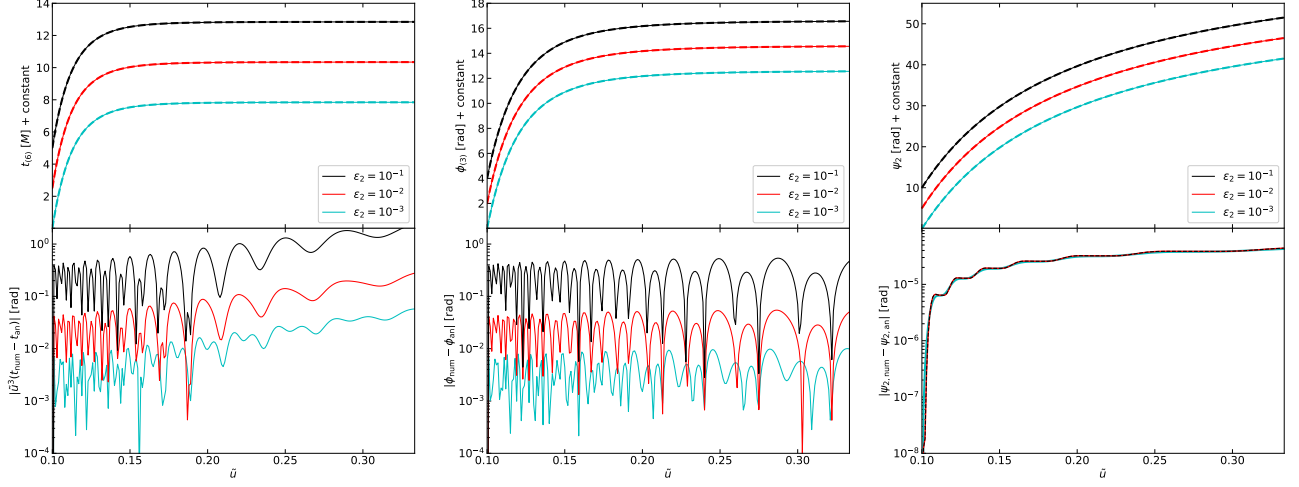


FIG. 3. Top Panel: Comparison of the numerical evolution (solid lines) of the time variable $t_{(6)}(\tilde{u}) = t(\tilde{u})/10^6$ (left), orbital phase $\phi_{(3)}(\tilde{u}) = \phi(\tilde{u})/10^3$ (middle), and precession phase $\psi_2(\tilde{u})$ to the analytic PN expressions (dashed lines) in Eq. (123), Eq. (124), and Eqs. (126) & (130), respectively. The dashed lines correspond to different values of the polar modulus ϵ_2 , specifically 10^{-3} (cyan), 10^{-2} (red), and 10^{-1} (black). The remaining parameters are held fixed at $\epsilon_1 = 10^{-3}$, $\alpha_2 = 0$, $\alpha_1 = \pi/2$, $\nu = 1/4$, and $Q_0 = M^3$. Bottom Panel: Dephasing in radians between the numerical evolution and analytic expressions. The dephasing in ψ_2 (bottom right) does not vary significantly for the values of ϵ_2 considered and it is mainly due to the PN truncation and the precession-average procedure.

where the Fourier phase is

$$\begin{aligned} \tilde{\Psi}_F &= 2\pi f t_c - 2\phi_c - \frac{\pi}{4} \\ &+ \frac{3}{128\nu(\pi M f)^{5/3}} \left[1 - \frac{5Q_0}{4M^3\nu} \sqrt{\frac{\pi}{5}} \epsilon_1^p \epsilon_2^q \mathcal{U}_{pq} (\pi M f)^{4/3} \right], \end{aligned} \quad (134)$$

and the Fourier amplitudes are

$$\mathcal{A}_m(f) = \sum_{k=0}^{k_{\max}} \frac{a_{k,k_{\max}}}{2} \{ A_{m,-2}[\psi_2(\tilde{u}_k)] + A_{m,-2}[\psi_2(\tilde{u}_{-k})] \}, \quad (135)$$

which are dependent on frequency through the SUA corrected \tilde{u}_k , specifically

$$\begin{aligned} \tilde{u}_k &= \tilde{u}(t_\star + kT_n) \\ &= (\pi M f)^{1/3} + 4k \sqrt{\frac{\nu}{15}} (\pi M f)^{7/6} \\ &\times \left[1 + \frac{Q_0}{16M^3\nu} \sqrt{\frac{\pi}{5}} \epsilon_1^p \epsilon_2^q \mathcal{U}_{pq} (\pi M f)^{4/3} \right]. \end{aligned} \quad (136)$$

In the above, the coefficients $a_{k,k_{\max}}$ satisfy the linear system of equations

$$\frac{(-i)^p}{2^p p!} = \sum_{k=0}^{k_{\max}} a_{k,k_{\max}} \frac{k^{2p}}{(2p)!}, \quad (137)$$

for $p \in 0, \dots, k_{\max}$. The value of k_{\max} is usually chosen based on the desired level of faithfulness when compared to numerical waveforms, as well as computational efficiency [48]. This completes the Fourier domain waveform for generic mass quadrupole effects.

To showcase these waveforms, we plot the amplitude functions $\mathcal{A}_m(f)$ in Fig. 4 for different values of the modulus parameters ϵ_m , specifically $\epsilon_m = 0$ (black lines) which corresponds to the spheroidal configuration, $\epsilon_m = 10^{-3}$ (red dashed lines), and $\epsilon_2 = 10^{-1} = 100\epsilon_1$. The amplitude functions are normalized such that $\mathcal{A}_m(f_{\text{low}}) = 1$, where $(\pi M f_{\text{low}})^{1/3} = 0.1$. For the spheroidal case, the inclination angle ι becomes a constant, and thus \mathcal{A}_0 also becomes constant with frequency. The amplitudes functions are generally modulated due to the precession of the orbital angular momentum, which defines the axis along which the GW amplitude is largest.

Finally, in Fig. 5 we plot the total phase difference between a spheroidal configuration and two configurations with $\epsilon_m = 10^{-3}$ (top panel) and $\epsilon_2 = 10^{-1} = 100\epsilon_1$ (bottom panel). The total phase of the waveform is found by

$$\tilde{\Psi}_T(f) = \tilde{\Psi}_F(f) + \arg \left[\sum_m \mathcal{A}_m(f) \right]. \quad (138)$$

The different lines in each panel correspond to different values of α_1 , while $\alpha_2 = 0$ for all cases.

As a simplistic but useful rule of thumb, an effect introducing a phase difference of 0.1 or greater is likely to substantially impact a matched-filter search, leading to a significant loss of detected events if the matched-

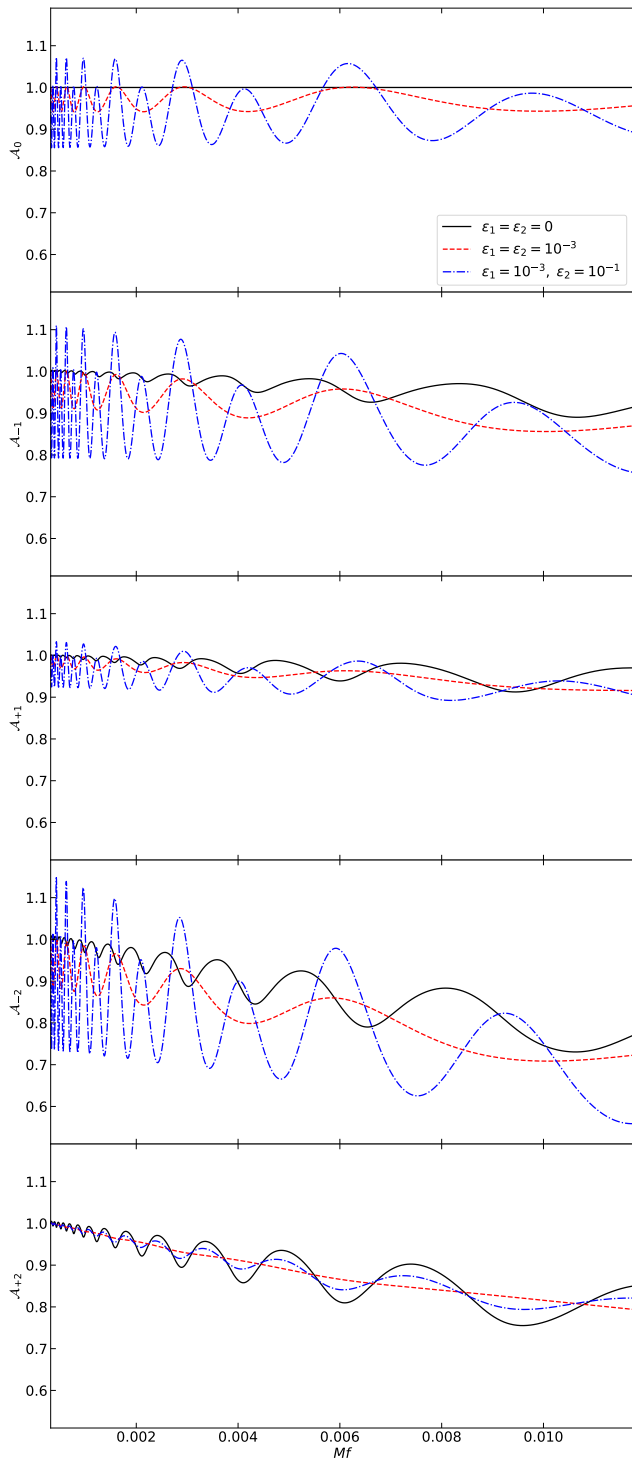


FIG. 4. Comparison of the waveform amplitudes \mathcal{A}_m from Eq. (135) for the spheroidal case (black), $\epsilon_1 = \epsilon_2 = 10^{-3}$ (red, dashed), and $\epsilon_1 = 10^{-3}, \epsilon_2 = 10^{-1}$ (blue, dot-dashed). The amplitudes are all normalized such that $\mathcal{A}_m = 1$ at the lowest frequency plotted.

filter search is done with waveforms that do not include these corrections [62]. Or, in other words, generally a

phase difference of 0.1 would in principle be observable by the LIGO and Virgo detectors at signal-to-noise ratio 10. Therefore, for all the cases shown in Fig. 5, the deviations from spheroidness could be detectable, although we stress that this naive estimates must be validated with a detailed parameter estimation study, also taking into account possible parameter correlations and systematic errors.

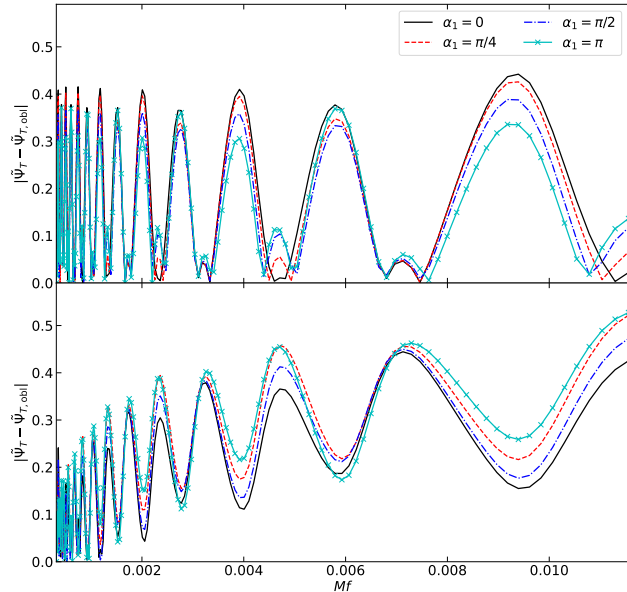


FIG. 5. Top Panel: Total GW phase difference between an oblate/prolate configuration and one with $\epsilon_1 = \epsilon_2 = 10^{-3}$. The polar phase $\alpha_2 = 0$, while the different lines correspond to different values of α_1 , namely 0 (black), $\pi/4$ (red, dashed), $\pi/2$ (blue, dot-dashed), and π (cyan, crossed). Bottom Panel: The same as the top panel but with $\epsilon_1 = 10^{-3}$ and $\epsilon_2 = 10^{-1}$.

V. DISCUSSION AND OUTLOOK

We have here developed the first analytic waveforms to model general mass quadrupole moment effects of compact objects. The waveforms are parameterized by the quadrupole parameter Q_0 corresponding to the oblate/prolate configuration, and the modulus ϵ_m and phase α_m parameters that describe deviations from spheroidness. The latter of these are generic enough for us to consider constraining non-axisymmetric configurations of compact objects. Besides considering non-axisymmetric bodies, the tools developed here can also be used to compute the leading-order correction for current quadrupole moments. This was partially addressed in Ref. [18] but only for the axisymmetric case and the main results were obtained in the EMRI limit. It should be stressed though that the generic mass quadrupole corrections considered here also break the equatorial symmetry and affect the waveform at a lower PN order rela-

tive to the axisymmetric \mathcal{S}_2 corrections considered in [18]. They should therefore be the leading-order signatures for generic objects without equatorial symmetry. Another natural extension of our work is to include the effect of the objects' angular momenta, which can give rise to a variety of phenomena (e.g., spin precession and coupling to the quadrupole moment).

A crucial aspect that we did not address in this paper is the extent with which GW detectors will be able to constrain or detect non-axisymmetric mass quadrupole moments. Based on a dephasing argument, we estimate that even small deviations from spheroidness might be measurable with current generation ground-based detectors. However, such an argument does not take into account the correlations among the physical parameters of the binary, or the possibility of degeneracies that would limit our ability to stringently constrain the additional quadrupole parameters. One degeneracy that can already be seen in the analysis carried out here is the fact that the waveforms depend on the components of the effective quadrupole moment tensor defined below Eq. (8), and not on the individual quadrupole moments of the objects. This is not surprising given that a similar situation happens when considering the leading PN spin and tidal corrections to the waveform [63]. In our specific case the situation is even worse, since the quadrupole tensor enters at the leading PN order through the *combination* $\epsilon_1^p \epsilon_2^q \mathcal{U}_{pq}$ in Eq. (134), so individual quadrupole components are degenerated. For example, based solely on the 2PN inspiral corrections, a (admittedly fine-tuned) model in which different components of the quadrupole moments conspire to give a negligible deviation from the standard Kerr case cannot be excluded. Higher-order PN corrections in the phase and amplitude can break this degeneracy.

A rough estimate of the constraints on generic quadrupolar deformations can come from measured upper bounds on the parametrized corrections, $\delta\phi_2$, to the 2PN coefficients. For the neutron-star binary GW170817 such constraints read $|\delta\phi_2| \lesssim 3.5$ at 90% confidence level [64]. For BH binaries, the latest bound obtained by combining all GWTC-3 events reads $|\delta\phi_2| \lesssim 0.1$ [65] (assuming the same type of deviations for all sources). These measurements could roughly translate into an upper bound on the combination $\epsilon_1^p \epsilon_2^q \mathcal{U}_{pq}$ (of both binary components) in Eq. (134). However, such bounds were derived without taking into account the amplitude corrections (see Eq. (135)) and the amplitude modulation (see Eq. (138)) found in this work, so a detailed analysis should be performed to obtain faithful constraints. At any rate, the order of magnitude of these constraints makes such parameter estimation a promising future avenue.

Another open question is how do the new parameters, specifically $[\epsilon_m, \alpha_m]$, map to the properties of compact objects. For BHs, $\epsilon_m = 0$, but in general this need not be true. In general, these parameters will be equation of state dependent. Having specific theoretical predic-

tions of these values for various astrophysical and exotic compact objects would allow one to map from generic constraints on the modulus and phase parameters to the physical set of parameters that characterizes the equation of state and structure of the bodies.

The calculations that we have carried out here are the first step toward more general investigations of the structure of compact objects, and we plan to investigate the above topics in future work.

ACKNOWLEDGMENTS

We acknowledge financial support provided under the European Union's H2020 ERC, Starting Grant agreement no. DarkGRA-757480. Computations were performed at Sapienza University of Rome on the Vera cluster of the Amaldi Research Center. This project has received funding from the European Union's Horizon 2020 research and innovation programme under the Marie Skłodowska-Curie grant agreement No 101007855. We also acknowledge support under the MIUR PRIN and FARE programmes (GW-NEXT, CUP: B84I20000100001, 2020KR4KN2), and from the Amaldi Research Center funded by the MIUR program "Dipartimento di Eccellenza" (CUP: B81I18001170001). This work is partially supported by the PRIN Grant 2020KR4KN2 "String Theory as a bridge between Gauge Theories and Quantum Gravity". R.B. acknowledges financial support provided by FCT – Fundação para a Ciência e a Tecnologia, I.P., under the Scientific Employment Stimulus – Individual Call – 2020.00470.CEECIND. The authors would like to acknowledge networking support by the GWverse COST Action CA16104, "Black holes, gravitational waves and fundamental physics."

Appendix A: Higher PN Effects

To complete the discussion in Sec. II A, we here provide some relevant PN quantities. We do not formally use these in the analysis presented in this paper. The 1PN and 2PN order corrections to the point particle Lagrangian in Eq. (5) are

$$\mathcal{L}_{1\text{PN}} = \frac{1 - 3\nu}{8} v^4 + \frac{M}{2r} \left[(3 + \nu) v^2 + \nu \dot{r}^2 - \frac{M}{r} \right], \quad (\text{A1})$$

$$\begin{aligned} \mathcal{L}_{2\text{PN}} = & \frac{1}{16} (1 - 7\nu + 13\nu^2) v^6 + \frac{M}{8r} [(7 - 12\nu - 9\nu^2) v^4 \\ & + (4 - 10\nu) \nu \dot{r}^2 v^2 + 3\nu^2 \dot{r}^4] + \frac{M^2}{2r^2} [(4 - 2\nu + \nu^2) v^2 \\ & + 3\nu(1 + \nu) \dot{r}^2] + \frac{M^3}{4r^3}, \end{aligned} \quad (\text{A2})$$

The PN corrections to the conserved orbital energy are

$$\begin{aligned} \frac{E_{1\text{PN}}}{\mu} &= \frac{3}{8}(1-3\nu)v^4 + \frac{1}{2}(3+\nu)v^2\frac{M}{r} + \frac{1}{2}\nu\frac{M}{r}\dot{r}^2 \\ &+ \frac{1}{2}\left(\frac{M}{r}\right)^2, \end{aligned} \quad (\text{A3})$$

$$\begin{aligned} \frac{E_{2\text{PN}}}{\mu} &= \frac{5}{16}(1-7\nu+13\nu^2)v^6 + \frac{1}{8}(21-23\nu-27\nu^2)\frac{M}{r}v^4 \\ &+ \frac{1}{4}\nu(1-15\nu)\frac{M}{r}v^2\dot{r}^2 - \frac{3}{8}\nu(1-3\nu)\frac{M}{r}\dot{r}^4 \\ &+ \frac{1}{8}(14-55\nu+4\nu^2)\left(\frac{M}{r}\right)^2v^2 \\ &+ \frac{1}{8}(4+69\nu+12\nu^2)\left(\frac{M}{r}\right)^2\dot{r}^2 - \frac{1}{4}(2+15\nu)\left(\frac{M}{r}\right)^3, \end{aligned} \quad (\text{A4})$$

$$E_{\text{SO}} = \frac{\mu}{r^2}\epsilon^{ijk}\Sigma^i n^j v^k, \quad (\text{A5})$$

$$E_{\text{SS}} = \frac{1}{r^3}\left[3(n^i S_1^i)(n^j S_2^j) - S_1^i S_2^i\right]. \quad (\text{A6})$$

Finally, the corrections to the conserved orbital angular momentum are

$$L_{1\text{PN}} = \frac{1}{2}v^2(1-3\nu) + (3+\nu)\frac{M}{r}, \quad (\text{A7})$$

$$\begin{aligned} L_{2\text{PN}} &= (1-7\nu+13\nu^2)\frac{3}{8}v^4 + (7-10\nu-9\nu^2)\frac{M}{2r}v^2 \\ &- \frac{1}{2}\nu(2+5\nu)\frac{M}{r}\dot{r}^2 + \frac{1}{4}(14-41\nu+4\nu^2)\left(\frac{M}{r}\right)^2, \end{aligned} \quad (\text{A8})$$

$$\begin{aligned} L_{\text{SO}}^i &= \frac{\mu}{M}\left[\frac{M}{r}\epsilon^{ijk}\epsilon^{kpq}n^j n^p(2S^q + \Sigma^q) \right. \\ &\left. - \frac{1}{2}\epsilon^{ijk}\epsilon^{kpq}v^j v^p \Sigma^q\right]. \end{aligned} \quad (\text{A9})$$

Appendix B: PN Quadrupole Coefficients

We here provide the coefficients of leading PN order corrections to various orbital quantities derived in Sec. III C and radiation reaction effects in Sec. IV A due to generic mass quadrupole moments. With $Q^a = [Q_0, Q_1^R, Q_1^I, Q_2^R, Q_2^I]$, the coefficients in Eqs. (109)-(110) are

$$\begin{aligned} \tilde{\mathcal{E}}_0 &= 6 + 2e_0^2 + 6(3 + e_0^2)\cos(2\iota) - (5 + 6e_0 + e_0^2)\cos[2(\iota - \omega)] + 10\cos(2\Omega) + 12e_0\cos(2\omega) + 2e_0^2\cos(2\omega) \\ &- 5\cos[2(\iota + \omega)] - 6e_0\cos[2(\iota + \omega)] - e_0^2\cos[2(\iota + \omega)], \end{aligned} \quad (\text{B1})$$

$$\tilde{\mathcal{E}}_1 = 8\sqrt{\frac{2}{3}}\sin\iota\left\{(5 + 6e_0 + e_0^2)\cos\Omega\sin(2\omega) + \cos\iota[-3(3 + e_0^2) + (5 + 6e_0 + e_0^2)\cos(2\omega)]\sin\Omega\right\}, \quad (\text{B2})$$

$$\tilde{\mathcal{E}}_2 = 2\sqrt{\frac{2}{3}}\sin\iota\left\{4\cos\iota[-3(3 + e_0^2) + (5 + 6e_0 + e_0^2)\cos(2\omega)]\cos\Omega - 4(5 + 6e_0 + e_0^2)\sin(2\omega)\sin\Omega\right\}, \quad (\text{B3})$$

$$\begin{aligned} \tilde{\mathcal{E}}_3 &= \frac{1}{\sqrt{6}}\left(-2\cos(2\Omega)\left\{2(1 + e_0)(5 + e_0)[3 + \cos(2\iota)]\cos(2\omega) + 12(3 + e_0^2)\sin^2\iota\right\} + 16(1 + e_0)(5 + e_0)\cos\iota\sin(2\omega)\sin(2\Omega)\right), \end{aligned} \quad (\text{B4})$$

$$\begin{aligned} \tilde{\mathcal{E}}_4 &= 2\sqrt{\frac{2}{3}}\left\{4(1 + e_0)(5 + e_0)\cos\iota\cos(2\Omega)\sin(2\omega) + [(1 + e_0)(5 + e_0)(3 + \cos(2\iota))\cos(2\omega) + 6(3 + e_0^2)\sin^2\iota]\sin(2\Omega)\right\}, \end{aligned} \quad (\text{B5})$$

$$\tilde{\mathcal{P}}_0 = (3 + e_0)^2[1 + 3\cos(2\iota)] + 2(1 + e_0)(5 + e_0)\cos(2\omega)\sin^2\iota, \quad (\text{B6})$$

$$\tilde{\mathcal{P}}_1 = 4\sqrt{\frac{2}{3}}\sin\iota\left\{(1 + e_0)(5 + e_0)\cos\Omega\sin(2\omega) + \cos\iota[-3(3 + e_0^2) + (1 + e_0)(5 + e_0)\cos(2\omega)]\sin\Omega\right\}, \quad (\text{B7})$$

$$\tilde{\mathcal{P}}_2 = \sqrt{\frac{2}{3}}\sin\iota\left\{4\cos\iota[-3(3 + e_0^2) + (1 + e_0)(5 + e_0)\cos(2\omega)]\cos\Omega - 4(1 + e_0)(5 + e_0)\sin(2\omega)\sin\Omega\right\}, \quad (\text{B8})$$

$$\begin{aligned} \tilde{\mathcal{P}}_3 &= \frac{1}{2\sqrt{6}}\left\{-2\cos(2\Omega)\left[2(1 + e_0)(5 + e_0)(3 + \cos(2\iota))\cos(2\omega) + 12(3 + e_0^2)\sin^2\iota\right] + 16(1 + e_0)(5 + e_0)\cos\iota\sin(2\omega)\sin(2\Omega)\right\}, \end{aligned} \quad (\text{B9})$$

$$\begin{aligned} \tilde{\mathcal{P}}_4 &= \sqrt{\frac{2}{3}}\left\{4(1 + e_0)(5 + e_0)\cos\iota\cos(2\Omega)\sin(2\omega) + [(1 + e_0)(5 + e_0)(3 + \cos(2\iota))\cos(2\omega) + 6(3 + e_0^2)\sin^2\iota]\sin(2\Omega)\right\}. \end{aligned} \quad (\text{B10})$$

The coefficients of the modified Kepler's third law in Eq. (112) are

$$\tilde{\Omega}_0 = 12 [3 + 9 \cos(2\iota) - \cos(2\omega) \sin^2 \iota] , \quad (\text{B11})$$

$$\tilde{\Omega}_1 = -4\sqrt{6} \{2 \cos \Omega \sin \iota \sin(2\omega) + [18 + \cos(2\omega)] \sin(2\iota) \sin \Omega\} , \quad (\text{B12})$$

$$\tilde{\Omega}_2 = 4\sqrt{6} \{36 \cos \iota \cos \Omega \sin \iota - [36 + \cos(2\omega)] \cos \Omega \sin(2\iota) + 2 \sin \iota \sin(2\omega) \sin \Omega\} \quad (\text{B13})$$

$$\tilde{\Omega}_3 = \sqrt{6} \{ \cos(2\Omega) [2(3 + \cos(2\iota)) \cos(2\omega) - 72 \sin^2 \iota] - 8 \cos \iota \sin(2\omega) \sin(2\Omega) \} , \quad (\text{B14})$$

$$\tilde{\Omega}_4 = 2\sqrt{6} \{ -4 \cos \iota \cos(2\Omega) \sin(2\omega) - [(3 + \cos(2\iota)) \cos(2\omega) - 36 \sin^2 \iota] \sin(2\Omega) \} . \quad (\text{B15})$$

Lastly, the coefficients for the orbital energy in Eq. (113) are

$$\tilde{E}_0 = 18 \cos(2\omega) \sin^2 \iota , \quad (\text{B16})$$

$$\tilde{E}_1 = 6\sqrt{6} [\cos(2\omega) \sin(2\iota) + 2 \cot \Omega \sin \iota \sin(2\omega)] \sin \Omega , \quad (\text{B17})$$

$$\tilde{E}_2 = 12\sqrt{6} \sin \iota [\cos \iota \cos(2\omega) \cos \Omega - 2 \cos \omega \sin \omega \sin \Omega] , \quad (\text{B18})$$

$$\tilde{E}_3 = 3\sqrt{6} \{ -[(3 + \cos(2\iota)) \cos(2\omega) \cos(2\Omega)] + 4 \cos \iota \sin(2\omega) \sin(2\Omega) \} , \quad (\text{B19})$$

$$\tilde{E}_4 = 3\sqrt{6} \{ 4 \cos \iota \cos(2\Omega) \sin(2\omega) + [3 + \cos(2\iota)] \cos(2\omega) \sin(2\Omega) \} . \quad (\text{B20})$$

The corrections to the evolution of the orbital frequency due to radiation reaction in Eq. (120) are

$$\tilde{U}_0 = -13 - 39 \cos(2\iota) + 98 \cos(2\omega) \sin^2 \iota , \quad (\text{B21})$$

$$\tilde{U}_1 = 2\sqrt{\frac{2}{3}} \{ 98 \cos \Omega \sin \iota \sin(2\omega) + [39 + 49 \cos(2\omega)] \sin(2\iota) \sin \Omega \} , \quad (\text{B22})$$

$$\tilde{U}_2 = 2\sqrt{\frac{2}{3}} \{ [39 + 49 \cos(2\omega)] \cos \Omega \sin(2\iota) - 98 \sin \iota \sin(2\omega) \sin \Omega \} , \quad (\text{B23})$$

$$\tilde{U}_3 = \sqrt{\frac{2}{3}} \{ \cos(2\Omega) [-49(3 + \cos(2\iota)) \cos(2\omega) + 78 \sin^2 \iota] + 196 \cos \iota \sin(2\omega) \sin(2\Omega) \} , \quad (\text{B24})$$

$$\tilde{U}_4 = \sqrt{\frac{2}{3}} \{ 196 \cos \iota \cos(2\Omega) \sin(2\omega) + [49(3 + \cos(2\iota)) \cos(2\omega) - 78 \sin^2 \iota] \sin(2\Omega) \} . \quad (\text{B25})$$

To obtain the coefficients \mathcal{U}_{pq} in Eq. (122), one has to compute the averages of the \tilde{U}_a coefficients listed above in a small $\epsilon_{1,2}$ expansion. The \tilde{U}_a are coupled to the quadrupole coefficients Q_a , and so each \tilde{U}_a must be expanded to different orders. For brevity, we only list the \mathcal{U}_{pq} up to linear order in the expansion. This means that \tilde{U}_0 must be computed to $\mathcal{O}(\epsilon_1, \epsilon_2)$ with remainders of order $\mathcal{O}(\epsilon_1^2, \epsilon_2^2, \epsilon_1 \epsilon_2)$, while all other \tilde{U}_a must be computed to $\mathcal{O}(\epsilon_1^0, \epsilon_2^0)$. The reason for this is that these are coupled to $Q_m^{R,I}$ which are already linear in ϵ_m , i.e. $Q_m^{R,I} \sim \epsilon_m Q_0$. Writing $\tilde{U}_0 = \tilde{U}_0^{(0)} + \epsilon_1 \tilde{U}_0^{(1)} + \epsilon_2 \tilde{U}_0^{(2)} + \mathcal{O}(\epsilon_1^2, \epsilon_2^2, \epsilon_1 \epsilon_2)$, the end results are

$$\mathcal{U}_{00} = -13 - 39 \cos(2\iota_0) + \frac{196}{\pi\zeta} \cos\left(\frac{\pi\zeta}{2} - 2\omega_0\right) \sin\left(\frac{\pi\zeta}{2}\right) \sin^2 \iota_0 \quad (\text{B26})$$

$$\mathcal{U}_{10} = \langle \tilde{U}_0^{(1)} \rangle_{\psi_2} + \sqrt{\frac{3}{2}} \left[\cos \alpha_1 \langle \tilde{U}_1 \rangle_{\psi_2} + \sin \alpha_1 \langle \tilde{U}_2 \rangle_{\psi_2} \right] \quad (\text{B27})$$

$$\mathcal{U}_{01} = \langle \tilde{U}_0^{(2)} \rangle_{\psi_2} + \sqrt{\frac{3}{2}} \left[\cos(2\alpha_2) \langle \tilde{U}_3 \rangle_{\psi_2} + \sin(2\alpha_2) \langle \tilde{U}_4 \rangle_{\psi_2} \right] \quad (\text{B28})$$

where $\zeta = [3 + 5 \cos(2\iota_0)] \sec \iota_0$, and

$$\begin{aligned} \langle \tilde{U}_0^{(1)} \rangle_{\psi_2} = & \frac{1}{2\pi\zeta^2} \left(\frac{49\zeta}{\zeta^2 - 4} \sin\left[\frac{\pi\zeta}{2}\right] \left\{ 8 \sin(2\iota_0) \left[(\zeta + 2) \sin\left(\frac{\pi\zeta}{2} - \Delta - 2\omega_0\right) + (\zeta - 2) \sin\left(\frac{\pi\zeta}{2} + \Delta - 2\omega_0\right) \right] \right. \right. \\ & + [7 + 4 \cos(2\iota_0) + 5 \cos(4\iota_0)] \sec \iota_0 \tan \iota_0 \left[(\zeta + 2) \sin\left(\frac{\pi\zeta}{2} - \Delta - 2\omega_0\right) - (\zeta - 2) \sin\left(\frac{\pi\zeta}{2} + \Delta - 2\omega_0\right) \right] \left. \right\} \\ & + 4 \sin \Delta [39\pi\zeta \sin\{2\iota_0\} - 49\{7 + 5 \cos(2\iota_0)\} \sin \iota_0 \{ \pi\zeta \cos(\pi\zeta - 2\omega_0) - \sin(\pi\zeta - 2\omega_0) - \sin(2\omega_0) \} \tan^2 \iota_0] \left. \right) , \end{aligned} \quad (\text{B29})$$

$$\begin{aligned} \langle \tilde{U}_0^{(2)} \rangle_{\psi_2} = & \frac{1}{8\pi\zeta(\zeta - 4)(\zeta + 4)} \{ 16\zeta \sin^2 \iota_0 [-39\pi\zeta(\zeta^2 - 16) + 784 \sin(\pi\zeta - 2\omega_0) + 784 \sin(2\omega_0)] \\ & + 98 \sec \iota_0 [\pi\zeta(\zeta^2 - 16)(23 + 36 \cos(2\iota_0) + 5 \cos(4\iota_0))] \cos(\pi\zeta - 2\omega_0) \\ & - 2 [-184 + 3\zeta^2 + 8(\zeta^2 - 36) \cos(2\iota_0) + 5(\zeta^2 - 8) \cos(4\iota_0)] [\sin(\pi\zeta - 2\omega_0) + \sin(2\omega_0)] \tan^2 \iota_0 \} , \end{aligned} \quad (\text{B30})$$

$$\begin{aligned} \langle \tilde{U}_1 \rangle_{\psi_2} = & -\frac{98}{\pi(\zeta^2 - 4)} \sqrt{\frac{2}{3}} \sin\left(\frac{\pi\zeta}{2}\right) \left\{ (\zeta + 2) [2 \sin \iota_0 + \sin(2\iota_0)] \sin\left(\alpha_2 - 2\omega_0 + \frac{\pi\zeta}{2}\right) \right. \\ & \left. - (\zeta - 2) [2 \sin \iota_0 - \sin(2\iota_0)] \sin\left(\alpha_2 + 2\omega_0 - \frac{\pi\zeta}{2}\right) \right\} \end{aligned} \quad (\text{B31})$$

$$\begin{aligned} \langle \tilde{U}_2 \rangle_{\psi_2} = & \frac{98}{\pi(\zeta^2 - 4)} \sqrt{\frac{2}{3}} \sin\left(\frac{\pi\zeta}{2}\right) \left\{ (\zeta + 2) [2 \sin \iota_0 + \sin(2\iota_0)] \cos\left(\alpha_2 - 2\omega_0 + \frac{\pi\zeta}{2}\right) \right. \\ & \left. - (\zeta - 2) [2 \sin \iota_0 - \sin(2\iota_0)] \cos\left(\alpha_2 + 2\omega_0 - \frac{\pi\zeta}{2}\right) \right\}, \end{aligned} \quad (\text{B32})$$

$$\begin{aligned} \langle \tilde{U}_3 \rangle_{\psi_2} = & -\frac{392}{\pi(\zeta^2 - 16)} \sqrt{\frac{2}{3}} \sin\left(\frac{\pi\zeta}{2}\right) \left[(\zeta + 4) \cos^4\left(\frac{\iota_0}{2}\right) \cos\left(2\alpha_2 - 2\omega_0 + \frac{\pi\zeta}{2}\right) \right. \\ & \left. + (\zeta - 4) \sin^4\left(\frac{\iota_0}{2}\right) \cos\left(2\alpha_2 + 2\omega_0 - \frac{\pi\zeta}{2}\right) \right], \end{aligned} \quad (\text{B33})$$

$$\begin{aligned} \langle \tilde{U}_4 \rangle_{\psi_2} = & -\frac{392}{\pi(\zeta^2 - 16)} \sqrt{\frac{2}{3}} \sin\left(\frac{\pi\zeta}{2}\right) \left[(\zeta + 4) \cos^4\left(\frac{\iota_0}{2}\right) \sin\left(2\alpha_2 - 2\omega_0 + \frac{\pi\zeta}{2}\right) \right. \\ & \left. + (\zeta - 4) \sin^4\left(\frac{\iota_0}{2}\right) \sin\left(2\alpha_2 + 2\omega_0 - \frac{\pi\zeta}{2}\right) \right]. \end{aligned} \quad (\text{B34})$$

Appendix C: Waveform Amplitudes

We here provide the waveform amplitudes $A_{m,n}^{\pm,\times}(\iota, \Omega)$ from Eq. (132).

$$A_{0,\pm 2} = 2\sqrt{\frac{6\pi}{5}} \sin^2 \iota, \quad (\text{C1})$$

$$A_{+1,+2} = -(A_{-1,-2})^\dagger = 8i\sqrt{\frac{\pi}{5}} e^{-i\Omega} \sin \iota \sin^2(\iota/2), \quad (\text{C2})$$

$$A_{+1,-2} = -(A_{-1,+2})^\dagger = -16i\sqrt{\frac{\pi}{5}} e^{-i\Omega} \sin(\iota/2) \cos^3(\iota/2), \quad (\text{C3})$$

$$A_{+2,+2} = (A_{-2,-2})^\dagger = -8\sqrt{\frac{\pi}{5}} e^{-2i\Omega} \sin^4(\iota/2), \quad (\text{C4})$$

$$A_{+2,-2} = (A_{-2,+2})^\dagger = -8\sqrt{\frac{\pi}{5}} e^{-2i\Omega} \cos^4(\iota/2). \quad (\text{C5})$$

-
- [1] J. D. Jackson, *Classical electrodynamics; 3rd ed.* (John Wiley & sons, New York, NY, 1999).
- [2] E. Poisson and C. Will, *Gravity: Newtonian, Post-Newtonian, Relativistic* (Cambridge University Press, Cambridge, UK, 2014).
- [3] B. Carter, Phys. Rev. Lett. **26**, 331 (1971).
- [4] S. W. Hawking, Commun. Math. Phys. **25**, 152 (1972).
- [5] D. C. Robinson, Phys. Rev. Lett. **34**, 905 (1975).
- [6] K. S. Thorne, Rev. Mod. Phys. **52**, 299 (1980).
- [7] S. W. Hawking and G. F. R. Ellis, *The Large Scale Structure of Space-Time*, Cambridge Monographs on Mathematical Physics (Cambridge University Press, 2011).
- [8] M. Heusler, Living Rev. Rel. **1**, 6 (1998).
- [9] P. T. Chrusciel, J. Lopes Costa, and M. Heusler, Living Rev. Rel. **15**, 7 (2012), arXiv:1205.6112 [gr-qc].
- [10] R. P. Geroch, J. Math. Phys. **11**, 2580 (1970).
- [11] R. O. Hansen, J. Math. Phys. **15**, 46 (1974).
- [12] B. Bonga and H. Yang, Phys. Rev. D **104**, 084040 (2021), arXiv:2106.08342 [gr-qc].
- [13] E. S. Ince, F. Barthelmes, S. Reißland, K. Elger, C. Förste, F. Flechtner, and H. Schuh, Earth System Science Data **11**, 647 (2019).
- [14] L. Lindblom and A. K. M. Masood-Ul-Alam, Communications in Mathematical Physics **162**, 123 (1994).
- [15] G. Raposo and P. Pani, Phys. Rev. D **102**, 044045 (2020), arXiv:2002.02555 [gr-qc].
- [16] G. Raposo, P. Pani, and R. Emparan, Phys. Rev. D **99**, 104050 (2019), arXiv:1812.07615 [gr-qc].
- [17] V. Cardoso and P. Pani, Living Rev. Rel. **22**, 4 (2019), arXiv:1904.05363 [gr-qc].
- [18] K. Fransen and D. R. Mayerson, (2022), arXiv:2201.03569 [gr-qc].
- [19] C. A. R. Herdeiro, J. Kunz, I. Perapechka, E. Radu, and Y. Shnir, Phys. Lett. B **812**, 136027 (2021), arXiv:2008.10608 [gr-qc].
- [20] I. Bena and D. R. Mayerson, Phys. Rev. Lett. **125**, 221602 (2020), arXiv:2006.10750 [hep-th].
- [21] M. Bianchi, D. Consoli, A. Grillo, J. F. Morales, P. Pani, and G. Raposo, Phys. Rev. Lett. **125**, 221601 (2020), arXiv:2007.01743 [hep-th].
- [22] I. Bena and D. R. Mayerson, JHEP **03**, 114 (2021), arXiv:2007.09152 [hep-th].

- [23] M. Bianchi, D. Consoli, A. Grillo, J. F. Morales, P. Pani, and G. Raposo, *JHEP* **01**, 003 (2021), arXiv:2008.01445 [hep-th].
- [24] I. Bah, I. Bena, P. Heidmann, Y. Li, and D. R. Mayerson, *JHEP* **10**, 138 (2021), arXiv:2104.10686 [hep-th].
- [25] F. D. Ryan, *Phys. Rev. D* **52**, 5707 (1995).
- [26] F. D. Ryan, *Phys. Rev. D* **56**, 1845 (1997).
- [27] D. Psaltis, *Living Rev. Rel.* **11**, 9 (2008), arXiv:0806.1531 [astro-ph].
- [28] J. R. Gair, M. Vallisneri, S. L. Larson, and J. G. Baker, *Living Rev. Rel.* **16**, 7 (2013), arXiv:1212.5575 [gr-qc].
- [29] N. Yunes and X. Siemens, *Living Rev. Relat.* **16**, 9 (2013), arXiv:1304.3473 [gr-qc].
- [30] E. Berti *et al.*, *Class. Quantum Grav.* **32**, 243001 (2015), arXiv:1501.07274 [gr-qc].
- [31] V. Cardoso and L. Gualtieri, *Class. Quant. Grav.* **33**, 174001 (2016), arXiv:1607.03133 [gr-qc].
- [32] L. Barack *et al.*, *Class. Quant. Grav.* **36**, 143001 (2019), arXiv:1806.05195 [gr-qc].
- [33] R. Abbott *et al.* (LIGO Scientific, Virgo), *Astrophys. J. Lett.* **896**, L44 (2020), arXiv:2006.12611 [astro-ph.HE].
- [34] R. Abbott *et al.* (LIGO Scientific, Virgo), *Phys. Rev. Lett.* **125**, 101102 (2020), arXiv:2009.01075 [gr-qc].
- [35] R. Abbott *et al.* (LIGO Scientific, Virgo), *Astrophys. J. Lett.* **900**, L13 (2020), arXiv:2009.01190 [astro-ph.HE].
- [36] K. Akiyama *et al.* (Event Horizon Telescope), *Astrophys. J. Lett.* **875**, L1 (2019), arXiv:1906.11238 [astro-ph.GA].
- [37] L. Blanchet, *Living Rev. Rel.* **17**, 2 (2014), arXiv:1310.1528 [gr-qc].
- [38] E. Poisson, *Phys. Rev.* **D57**, 5287 (1998), arXiv:gr-qc/9709032 [gr-qc].
- [39] G. Pappas and T. P. Sotiriou, *Mon. Not. Roy. Astron. Soc.* **453**, 2862 (2015), arXiv:1505.02882 [gr-qc].
- [40] N. V. Krishnendu, K. G. Arun, and C. K. Mishra, *Phys. Rev. Lett.* **119**, 091101 (2017), arXiv:1701.06318 [gr-qc].
- [41] N. V. Krishnendu, C. K. Mishra, and K. G. Arun, *Phys. Rev. D* **99**, 064008 (2019), arXiv:1811.00317 [gr-qc].
- [42] S. Kasta, A. Gupta, K. G. Arun, B. S. Sathyaprakash, and C. Van Den Broeck, *Phys. Rev. D* **98**, 124033 (2018), arXiv:1809.10465 [gr-qc].
- [43] S. Kasta, A. Gupta, K. G. Arun, B. S. Sathyaprakash, and C. Van Den Broeck, *Phys. Rev. D* **100**, 044007 (2019), arXiv:1905.07277 [gr-qc].
- [44] N. V. Krishnendu and A. B. Yelkar, *Class. Quant. Grav.* **37**, 205019 (2020), arXiv:1904.12712 [gr-qc].
- [45] L. Barack and C. Cutler, *Phys. Rev. D* **75**, 042003 (2007), arXiv:gr-qc/0612029.
- [46] S. Babak, J. Gair, A. Sesana, E. Barausse, C. F. Sopuerta, C. P. L. Berry, E. Berti, P. Amaro-Seoane, A. Petiteau, and A. Klein, *Phys. Rev. D* **95**, 103012 (2017), arXiv:1703.09722 [gr-qc].
- [47] C. M. Bender and S. A. Orszag, *Advanced mathematical methods for scientists and engineers 1, Asymptotic methods and perturbation theory* (Springer, New York, 1999).
- [48] A. Klein, N. Cornish, and N. Yunes, *Phys. Rev. D* **90**, 124029 (2014), arXiv:1408.5158 [gr-qc].
- [49] T. Abdelsalhin, L. Gualtieri, and P. Pani, *Phys. Rev. D* **98**, 104046 (2018), arXiv:1805.01487 [gr-qc].
- [50] K. S. Thorne, *Rev. Mod. Phys.* **52**, 299 (1980).
- [51] L. E. Kidder, C. M. Will, and A. G. Wiseman, *Phys. Rev. D* **47**, R4183 (1993).
- [52] J. Steinhoff, *Annalen Phys.* **523**, 296 (2011), arXiv:1106.4203 [gr-qc].
- [53] K. Chatziioannou, A. Klein, N. Cornish, and N. Yunes, *Phys. Rev. Lett.* **118**, 051101 (2017), arXiv:1606.03117 [gr-qc].
- [54] K. Chatziioannou, A. Klein, N. Yunes, and N. Cornish, *Phys. Rev. D* **95**, 104004 (2017), arXiv:1703.03967 [gr-qc].
- [55] E. Racine, *Phys. Rev. D* **78**, 044021 (2008), arXiv:0803.1820 [gr-qc].
- [56] M. Kesden, D. Gerosa, R. O’Shaughnessy, E. Berti, and U. Sperhake, *Phys. Rev. Lett.* **114**, 081103 (2015), arXiv:1411.0674 [gr-qc].
- [57] J. Steinhoff, T. Hinderer, A. Buonanno, and A. Taracchini, *Phys. Rev.* **D94**, 104028 (2016), arXiv:1608.01907 [gr-qc].
- [58] V. Cardoso, M. Kimura, A. Maselli, and L. Senatore, *Phys. Rev. Lett.* **121**, 251105 (2018), arXiv:1808.08962 [gr-qc].
- [59] N. Sennett, R. Brito, A. Buonanno, V. Gorbenko, and L. Senatore, *Phys. Rev. D* **102**, 044056 (2020), arXiv:1912.09917 [gr-qc].
- [60] C. Konigsdorffer and A. Gopakumar, *Phys. Rev. D* **73**, 124012 (2006), arXiv:gr-qc/0603056.
- [61] T. Mora and C. M. Will, *Phys. Rev.* **D69**, 104021 (2004), [Erratum: *Phys. Rev.* **D71**, 129901(2005)], arXiv:gr-qc/0312082 [gr-qc].
- [62] L. Lindblom, B. J. Owen, and D. A. Brown, *Phys. Rev. D* **78**, 124020 (2008), arXiv:0809.3844 [gr-qc].
- [63] E. E. Flanagan and T. Hinderer, *Phys. Rev.* **D77**, 021502 (2008), arXiv:0709.1915 [astro-ph].
- [64] B. P. Abbott *et al.* (LIGO Scientific, Virgo), *Phys. Rev. Lett.* **123**, 011102 (2019), arXiv:1811.00364 [gr-qc].
- [65] R. Abbott *et al.* (LIGO Scientific, VIRGO, KAGRA), (2021), arXiv:2112.06861 [gr-qc].